Jouni Huopana
Matilaisentie 2 A 1
90570 Oulu
Finland
044–2800101

DESIGN OF PRECISION ALIGNMENT OF COMPACT LINEAR COLLIDERS ACCELERATING STRUCTURES

Master's Thesis, which subject has been approved by the Department of Mechanical Engineering in the University of Oulu.
August 31, 2007

Supervisor: Prof. Stig-Göran Sjölind
Instructor: Mauro Taborelli

UNIVERSITY OF OULU ABSTRACT OF THE MASTER'S THESIS

Author:	Jouni Huopana	
Title:	Design of Precision Alignment of Compact Linear Collider Accelerating Structures	
Date:	October 3, 2007	**Number of pages:** 75 + 14
Department:	Mechanical Engineering	
Professorship:	Engineering Mechanics	
Supervisor:	Prof. Stig-Göran Sjölind	
Instructor:	Dr. Phys. Mauro Taborelli	

This thesis evaluates different assembly methods for particle accelerator called Compact Linear Colliders (CLIC)accelerating components. This work focuses on the definition of a strategy and mechanical design for the assembly of four quadrants in radial and longitudinal direction. The study takes into account the constraints specified by the various aspects of the physics involved in the application of such accelerating structures. The possible deformations due to a kinematic or elastic assembly and its influence on the final accuracy are calculated. Also the work considers the effect of a moderate temperature rise due to the steady state heating during machine operation and other loads due to the function of the machine. Accelerating structures must be aligned around the beam axis with a transversal accuracy of +/-0.003 mm and longitudinal accuracy of +/-0.01 mm over the length of a single module. This requirement includes the accuracy of the parts to be manufactured and the precision of the assembly of the various components.

There were three main assemblies types studied; pin assembly, sphere assembly and averaging shape assembly. A program was written to compare the different methods with respect to the mechanical differences and manufacturing tolerances. In addition, the effects of different kind of loads affecting the structures were studied via FEM-programs. These results were then used to compare and evaluate the different mechanical configurations mechanical behavior and the effects on the final results.

The best assembly method can be chosen by using these comparing results. The results indicated that with the averaging shapes it is possible to exploit the elastic behavior of the structure to achieve the final assembly accuracy. This accuracy is also acceptable for the accelerating structures.

Keywords: assembly techniques, FEM-simulations, high presicion mechanics

OULUN YLIOPISTO DIPLOMITYÖN TIIVISTELMÄ

Tekijä:	Jouni Huopana		
Työn nimi:	Lineaarisen hiukkaskiihdyttimen kiihdytinkomponenttien tarkkuuskokoonpanon suunnittelu		
Päivämäärä:	3.10.2007	**Sivuja:**	75 + 14
Osasto:	Konetekniikan osasto		
Professuuri:	Teknillinen mekaniikka		
Työn valvoja:	Prof. Stig-Göran Sjölind		
Työn ohjaaja:	FT. Mauro Taborelli		

Tässä työssä tutkitaan erilaisia kokoonpanomenetelmiä lineaarisen hiukkaskiihdyttimen kiihdytin komponenteille. Tämä työ keskittyy mekaniikan suunnitteluun kokoonpanolle, joka koostuu neljästä neljänneksestä ja näiden asemoinnista pitkittäis- ja säteissuunnassa. Työssä otetaan huomioon rakenteeseen vaikuttavat fysikaaliset ilmiöt, jotka aiheutuvat hiukkaskiihdyttimen käytöstä. Lisäksi huomioidaan kinemaattisten ja elastisten kokoonpanotekniikoiden vaikutus rakenteen käyttäytymiseen ja lopulliseen tarkkuuteen. Myös lämpötilan nousun vaikutukset otetaan huomioon, jotka syntyvät kiihdyttimen käytöstä. Komponentit on asemoitava hiukkassäteen poikittaissuunnassa +/-0.003 mm tarkkuudella ja hiukkassäteen suunnassa +/-0.01 mm tarkkuudella, yhden rakennemoduulin matkalla (n. 2 m). Nämä toleranssirajat pitävät sisällään yksittäisen komponentin valmistuksesta ja asemoinnista johtuvat toleranssirajat.

Työssä tutkittiin kolmea eri kokoonpanotekniikkaa; sylinteritappien käyttöä, tarkkuuskuulien käyttöä, sekä koneistettuja muotoja. Näitä vertaillaan toisiinsa käyttämällä MATLAB-koodia, jossa huomioidaan eri kokoonpano vaihtoehtojen eroavaisuudet mekaniikassa sekä valmistustoleranssien vaikutus. Lisäksi rakenteeseen vaikuttavien erilaisten kuormitusten vaikusta tarkastellaan elementtimenetelmäohjelmistojen avulla. Näitä tuloksia tutkimalla saadaan käsitys rakenteen mekaanisesta käyttäytymisestä ja kokoonpanon lopulliseen tarkkuuteen vaikuttavista tekijöistä.

Vertailevien tulosten perusteella voitiin todeta koneistettujen muotojen olevan tarkin kokoonpanomenetelmä. Tulokset osoittavat, että käytettäessä koneistettuja muotoja, voidaan hyödyntää rakenteen elastisia ominaisuuksia lopullisen asemointitarkkuuden saavuttamiseksi. Tämä tarkkuus on riittävä hiukkaskiihdyttimen kokoonpanolle.

Avainsanat: kokoonpanotekniikat, FEM-simulaatiot, tarkkuusmekaniikka

Acknowledgements

I would like to express my gratitude to Helsinki Institute of Physics (HIP) and Finnish Technology Institute (VTT) for the opportunity to work in CERN for this work. I am also grateful for Prof. Stig Göran Sjölind for his guidance and for Dr(Tech) Kimmo K. Mäkelä (VTT) for his comments for the work. I would like to thank Dr. Phys. Mauro Taborelli (CERN) and Kenneth Österberg (HIP) for their assistance during this work and Hannu Koivurova who also reviewed the work. Also the whole precision mechanics team at Oulu and CLIC-team at CERN deserve thanks for the support and help in the process of this work.

Oulu, September 21, 2007

Jouni Huopana

Contents

Notations

a	manufacturing tolerance	[μm]
α	thermal diffusivity	[s]
b_i	body force	
D	Elasticity matrix	
δ	gap	[mm]
E	Young's modulus	[GPa]
ϵ	strain	
$\{F\}$	external force vector	
F_n	normal force	
γ	rotation	
I	identity matrix	
$[K]$	stiffness matrix	
k_n	normal contact stifness	
λ	Lagrange multiplier	
N_i	shape function	
ν	Poison's coefficient	
∇	operator	

$[M]$	mass matrix	
μ	mean	
ω	eigenfrequency	[Hz]
q_i	nodal forces	
R	thermal conductivity	
$\mathbf{S}$	linear operator	
$\sigma_{x,y}$	stress	[MPa]
σ_{dev}	standard deviation	
T	temperature	[C°]
ΔT	temperature change	[C°]
t	time	[s]
τ	thermal relaxation time	[s]
τ_{xy}	shear stress	[MPa]
u	displacement vector	
V	volume	[m^3]
v	thermal wave speed	[m/s]
$\{v\}$	thermal diffusivity	
x_k	kth coordinate value	[mm]
x_{pen}	penetratio	

Abbreviations

CERN	European Organization for Nuclear Research
CLIC	Compact LInear Collider
CMM	Contact Measuring Machine
DOF	Degrees Of Freedom
FEM	Finite Element Method
LHC	Large Hardon Collider
UHV	Ultra High Vacuum

List of Figures

List of Tables

Chapter 1

Introduction

The curiosities of many modern scientists and physicist have been fixed towards the very essence of material for decades. To learn more about atoms, electrons, quarks, and the particles that still eludes us. To study these basic building blocks of universe the particle collider technology has been developed. Accelerators induce high energy to subatomic particles. These particles are then collided. From this collition other particles can be formed and detected. The gathered data can be used to study the nature of particles and matter. There has been many techniques and approaches through time to do this and whenever there has been an accelerator built, there has always been a need to build a more powerful accelerator or an accelerator that collides different kinds of particles to study the unknown territory that has been left in the shadows by the previous technology. At this time the Large Hardon Collider (LHC) is closing completion therefore the technology for the next generation of accelerator is under development to response the results and needs that the LHC will present. The idea for LHC emerged 22 years ago and it has been under construction for the last twelve years. LHC will be 27 km long circular accelerator and will collide protons at an energy of 14 TeV. The completion of LHC is scheduled to spring of 2008. [1, 2]

> A TeV is a unit of energy used in particle physics. 1 TeV is about the energy of motion of a flying mosquito. What makes the LHC so extraordinary is that it squeezes energy into a space about a million million times smaller than a mosquito. [1]

1.1 Compact Linear Collider

The first idea to use linear acceleration was presented by Rolf Wideröe in 1928 [3]. The development of the idea stayed dormant until the improvements in microwave technologies in radar technology in World War II opened new possibilities for the linear accelerator. The Compact Linear Collider (CLIC) is a next generation linear positron-electron collider. With its current parameters the total length of the collider is close to 50 km [4]. As the LHC approaches completion, many of the world's physicists agree that to achieve the needed energy level in the next accelerator, the accelerator should be a linear one and that CLIC might be an option to meet this demand. This is mainly because the LHC and its predecessors have been circular accelerators which means that the accelerated particle on its circular path creates synchrotron radiation. The limits of this type of technology can clearly been seen at LHC, as it is the largest superconducting circular accelerator that has been built. The linear collider does not suffer from synchrotron radiation, but as it is linear, the possibility to use the same route to accelerate the particles does not exist. This means that to achieve the needed energy levels for the collision the accelerating gradient must be as high at it can. These high gradient particle beams induce multiple constraints and loads to the accelerating structures. The design of the CLIC is a module based system. Each module includes everything that is needed for the function of the accelerator. The length of a single module is two meters. [5–7]

1.1.1 Accelerating structures

The main accelerating structure used in this thesis is an accelerating structure which is compiled from four quadrants. This structure was developed to improve the disk assembly used previously in linear accelerators. The benefits of this structure are simpler manufacturing and a design that has damping, using slots and radial waveguides. Also this structure can be optimized for better performance and efficiency. The structures four quadrants have similar geometries. The particle beam will be accelerated from the center of the structure, illustrated in figure 1, where one of the quadrants has been removed. The example structure in this thesis is a 300 mm quadrant with a square cross-section of 50 mm x 50 mm. Figure 2 explains the different parts and shapes of the geometry. The final design will be, that in one module will consist from four assemblies placed one after another, making the total number of quadrants in one module to sixteen. The number of quadrants in CLIC can be close to 250000, depending on the design and configuration. [8]

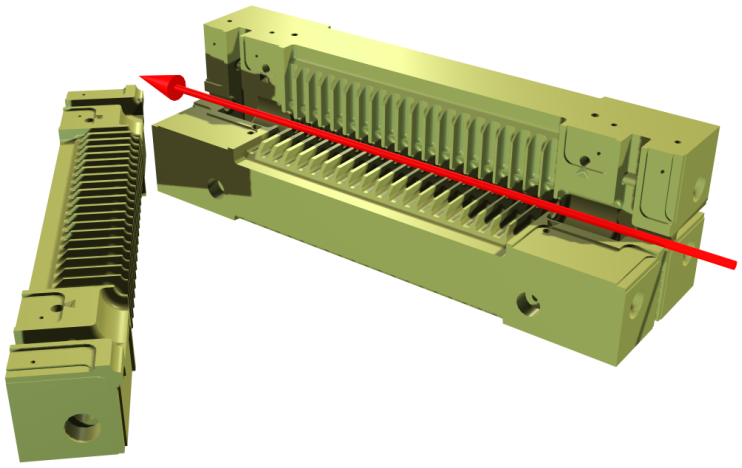

Figure 1. Accelerating structure and the path of the beam

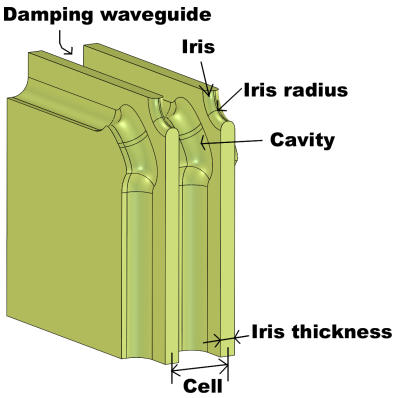

Figure 2. Geometry and its different shapes of the structure

This work focuses on the definition of a strategy and mechanical design for the assembly of four quadrants in radial and longitudinal direction. In addition the design for the longitudinal alignment with the next set of quadrants is considered. The study will take into account the various constraints from many aspects of the physics involved in the application of the accelerating structures. The possible deformations due to assembly techniques and its influence on the final accuracy are calculated. This work also considers the effect of a moderate temperature rise due to the steady state heating during machine operation and other loads due to the function of the machine. Accelerating structures must be aligned around the beam axis with a transversal accuracy of +/-0.003 mm and longitudinal accuracy of +/-0.01 mm over the length of a single module. This requirement includes the accuracy of the parts to be manufactured and the precision of the assembly of the various components. Also the accuracy of the assembly should not be influenced by the installation of the parts to the module and it should be assumed that the installed parts will not move during the operation of the machine. The requirements from the point of view of the radio-frequency imply that the quadrants are in contact at least for the surfaces facing the beam, so that no sharp steps are apparent on those surfaces. The materials to be used for the positioning features should be compatible with Ultra-High-Vacuum technology. The vacuum is needed to ensure that the accelerated particle beam could travel without unnecessary interactions. As the quadrant assembly is placed inside a vacuum, high friction will prevent any movement of the parts. The assembly should also be designed in a way, that the accuracy can be verified by conventional

metrology tools, as CMM (contact Measuring Machine). For the CLIC machine the assembly does not need to be reversible, since dismounting of the various quadrants is not foreseen, however this option is extremely convenient for the present research and development phase of prototypes.

Chapter 2

Assembly techniques

2.1 Design methods for a high accuracy assembly

The required tolerances for the accelerator set the need for high precision assembly. However, so far the different assemblies have only been proven to achieve an accuracy which is not at acceptable level. To have comparable data between different assembly methods is crucial, when choosing the final design. Thefore there must be an attempt to study the different techniques of assembly to overcome the tolerance limitations. It should also be noted that the manufacturing tolerances, which usually directly correspond to the accuracy level of the final assembly, are very high.

There have been significant steps forward, considering the assembly accuracy of two parts, in the resent years. The development has been pushed forward by growing demand for higher accuracy and the development of various manufacturing technologies. Most of the assembly techniques emphasize the repeatable accuracy of the design. To have precision to one-time assembly is to design the parts so, that the design compensates the precision of the machining and the effects of the operation of the accelerator. Machining precision usually defines the final precision of the assembly. It is also good to notice, that usually all the theoretical and prototype assemblies consider the precision alignment of two parts. There are four main methods of alignment which will be explained; elastic averaging, pinned joints, kinematic constraints and quasi-kinematic constraints.

The differences in repeatability of these methods can be seen in table 1. [9, 10]

Table 1. Achievable repeatability of assembly methods

	Pinned joints	Elastic averaging	Kinematic ass.	Q.-kinematic ass.
Error [μm]	5 μm	5 μm	0,03 μm	0,15 μm

Accuracy is the maximum rotational and transitional error between any two points and this should not be confused with *repetition accuracy* or *repeatability* that shows the error between each assembly attempts. [11]

2.1.1 Elastic averaging

Elastic averaging is based on elastic deformation between the contact bodies. When a repetitive shape is introduced to the surface of an object and a negation of this shape is located in the opposite body, the multiple contacts create an averaging phenomenon that increases the overall accuracy of the coupling. The down side of using elastic deformation, as a part of the assembly mechanism, is that whenever a contact is made there can be some plastic deformation that occurs due to high stress in small contact areas. This lowers the repetition accuracy and has a clear effect on the surface quality of the parts. To improve this design a third element can be introduced. If the repetitive pattern in between the contact surfaces is designed, so that there is a space between the parts, the plastic deformation can be lower by using a softer element between the contact surfaces. This element would therefore deform more easily than the parts of the assembly. This would increase the repetition accuracy of the assembly and protect the surface of the parts. Due to relatively large contact areas, elastic averaging joint can withstand high load by distributing the created pressure to large areas. The principle is shown in figure 3. [12]

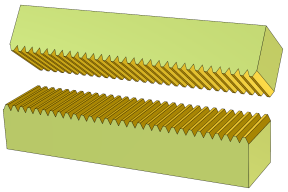

Figure 3. Principle of elastic averaging

2.1.2 Pinned joints

Pinned joint is the most basic method of accurate assembly. The idea is to use high accuracy pins in high accuracy holes to create a fully constraint pair. This method is however the most inaccurate in repetitive assembly and it is heavily depended on the machining accuracy. The design of a pinned joined is very simple. It uses two pins per contact area and therefore constrains planar movement. The principle is shown in figure 4. The load carrying capability is limited mainly by the shear strength of the pins. The loads that are parallel to the pins, are carried by the interface surfaces of the assembly. This method should not be confused with the kinematic method of using pins as an alignment feature.

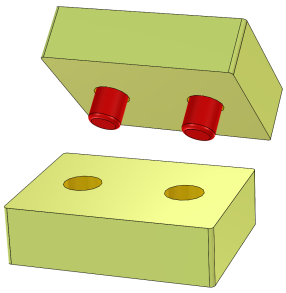

Figure 4. Pinned joint

2.1.3 Kinematic joints

Kinematic joints have were developed about 200 years ago and they have been very effective to reproduce a high repetition accuracy. This method is based on an idea to create a fully constrained coupling. This means that when the assembly is done, it has three rotational and three linear movements constrained. If one of these constraints is removed the joint will have a one degree of freedom.(Figure 5) Kinematic coupling can increase the precision of the assembly of designed properly. It is only possible to reduce the effects of the machining on certain areas of the parts. The loading capability is relatively small with kinematic couplings. The small areas of contact in each support causes high stresses even with small forces and the loads which are parallel to the surface are carried only if the compressive force is big enough. [13, 14]

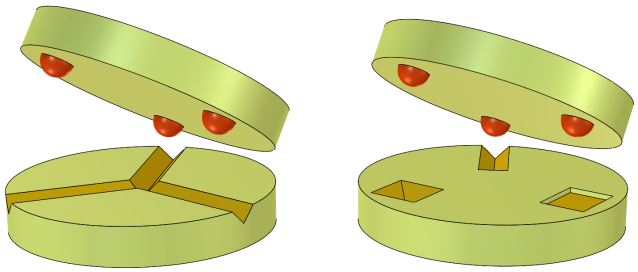

Figure 5. Two kinematic couplings

2.1.4 Quasi-kinematic coupling

Quasi-kinematic coupling was developed to improve the load carrying capability of kinematic joints. This was achieved by making the fully constrained assembly slightly over constrained. This happens when for example a sphere is inserted into a cone which has some of the material removed for either side. The sphere is in line contact with the cone, but if a compression force is applied to the sphere, it can move slightly due to the elastic deformation, to the direction of the removed material. With this method it has been shown that it is possible to create an assembly with better than 10 μm repetition accuracy, but only with a proper design. Also the load carrying capability is higher compared to the kinematic joints, but if the compression force is increased much, the elastic deformation can turn into plastic. [9, 15]

Chapter 3

Design of a single quadrant and the assembly

In the course of development of CLIC and the accelerating components there has been prototypes that have been used to study the capabilities of the structure. These parts have been assembled with kinematic constraints. The accuracy of such systems are and have been very sensitive to machining accuracy. To achieve the required tolerance in the final assembly it should be understood that the final tolerance range of the assembly is a combination of various tolerances which are due to the machining and assembly of the quadrants. To achieve such high accuracy as much as possible of the manufacturing should be considered in the final design. Including the manufacturing temperature, stability of the milling machine and the final assembly in vacuum.

To have efficient and reliable assembly, the number of the parts in the assembly should be kept as low as possible. As the number of the assemblies is very high in the whole accelerator, there should be effort to avoid too complicated methods of an assembly and any methods which require adjustments. It is also preferable to make the assembly features such that it is difficult to make incorrect assembly.

The first assembly technique that has been applied was a kinematic assembly that was designed with pins. The assembly is fairly capable to compensate thermal expansion. This was done by using pins close to the beam axis which were parallel to the beam and to prevent axial movement two pins were set perpendicular to the beam axis, making the assembly slightly over constrained kinematicly.

It should be considered that even this has been included to the design, the thermal expansions causes maximum ΔT 10°C. This difference of temperature causes a maximum of 0.004 mm of elongation for a beam structure (l=$l_0\alpha\Delta$T). [16] The calculations show that kinematic constraint is directly related to the manufacturing accuracy and is highly dependent on the screw forces. [17]

Another kinematic assembly has been used is also studied. The design uses the idea of zero Degrees Of Freedom (DOF). This is achieved by using two spheres as the main alignment system. The two spheres are placed close to the beam axis and tightened from as close as possible to achieve high accuracy and low leveraging effect from the screw. The first sphere is set into a prism shaped pocket which therefore excludes all the movement for the sphere, except rotations. This fixes the two parts of the assembly only allowing one rotational DOF. The other sphere is located in a V-groove so that the radial movement between two parts is locked. The needed compression forces are studied and the contacts between the sphere and grooves as well as the effects of the tolerances to such a structure.

The elastic averaging was adapted so that the number of surface contacts would be increased during the assembly. The higher number in contacts would then average the joint between two parts. All the parts were designed to be manufactured from copper. The averaging shapes were designed so that the most critical tolerance was with the shortest leverage. The joining of the parts was made with standard screws and the effect of the tightening was also studied. It can be seen from the results that the assembly is as accurate as the individual part. Also the contact regions are studied to define the needed forces for the assembly as well as the temperature effects of steady-state heating.

Quasi-kinematic couplings can be described as a combination of kinematic couplings and elastic averaging. A lot of research relating to this design has been done by Culpepper [9]. These couplings are based to the same idea of eliminating the degrees of freedom as kinematic couplings, but the differences is that by right design the coupling has controlled elastic and plastic deformation. These combined features give the joint the accuracy of kinematic coupling and the load carrying abilities of elastic averaging. However this assembly technique can diminish the machining accuracy only on certain areas as does the kinematic couplings. The main difference compared to the kinematic coupling is the higher repetition accuracy.

3.1 Tolerances

The accelerator structure's tolerances are based on beam dynamics of the particle beam. Misalignment causes the beam to deviate form its intended path. Misalignment causes a drop to the efficiency of the machine and in worse cases can damage the structure. The biggest issue is that the cells of the aligned structures must be in longitudinal direction in $\pm 1\mu$m or the beam can divert from its intended path. (Figure 6)

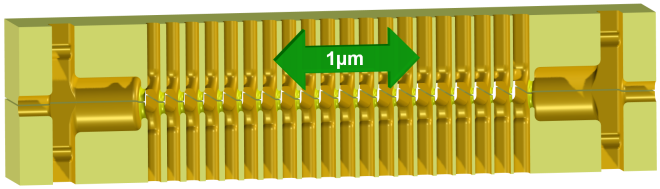

Figure 6. Tolerances z-axis

Also the transversal direction to the beam axis is sensitive to misalignment but the assembly can tolerate $\pm 3\mu$m misalignment. (Figure 7)

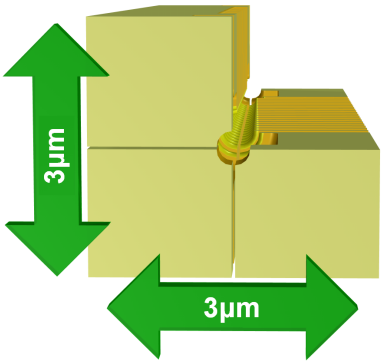

Figure 7. Transversal tolerances

The manufacturing tolerances of this kind of high precision parts are crucial considering the final accuracy of the parts and are the main contributor in the tolerance scale.

3.2 Materials

The best candidate for a material to be used to manufacture the accelerating structures is oxygen free copper. The main reasons for this are the high electrical conductivity and the material purity. This kind of copper is highly suitable for example for semiconductors and high energy physics applications. Also copper has a high thermal conductivity, fully compatible with high-vacuum applications and with a proper manufacturing, high surface quality. The alignment elements are manufactured from stainless steel. The mechanical properties used can be seen in table 2. [18, 19]

Table 2. Material properties

Properties	Copper	Structural Steel
Structural		
Young's Modulus	110 GPa	200 GPa
Poisson's Ratio	0,34	0,3
Density	8300 kg/m^3	7850 kg/m^3
Thermal Expansion	1,8·10^{-5} 1/°C	1,2·10^{-5} 1/°C
Tensile Yield Strength	280 MPa	250 MPa
Compressive Yield Strength	280 MPa	250 MPa
Tensile Ultimate Strength	430 MPa	460 MPa
Thermal		
Thermal Conductivity	0,401 W/ mm °C	6,05·10^{-2} W/ mm °C
Specific Heat	385 J/kg °C	434 J/kg °C

3.3 Loads and constraints

3.3.1 Assembly loads

Mechanical loads that affect the fully assembled quadrants are mostly due to mechanical contact with other parts. The amount that is given by earth gravitational acceleration is considered negligible. Main contributors for loads are bolts that are tightened to keep the quadrants together and due to this tightening the Hertzian pressure of alignment features causes stresses. The effects of the bolts can be simulated with ANSYS finite element program (Figure 8). Also the electric currents which are generated by the magnetic fields cause steady-state heating. The effects of the heating can be also studied with ANSYS.

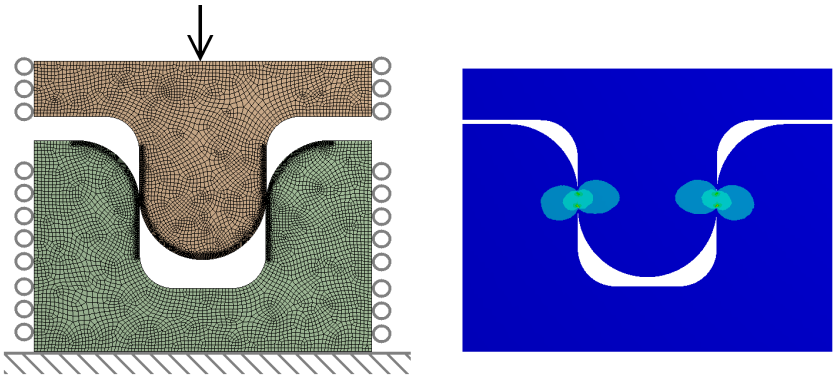

Figure 8. View from a finite element program

Table 3. Loads, constraints and effects

Load	Constraint	Effect
Electro-Magneticfield	Temperature change	Surface currents induces pulsed surface heating, which transforms to steady-state heating. Heating causes thermal expansion, for Cu 18 μm/m·°C
Alignment	Applied force	Bolt forces, elastic deformation, stresses, σ=Eϵ
Gravity	Body force,	Static loading, deflection
Cooling	Temperature gradient,	Thermal expansion,
	vibration	stability
		eigenfrequencies
Instrumentation	Applied force	Stability
		deflections
		static loading

The accuracy calculations were conducted with MATLAB version 7.3.0.267 (r2006b). The program was chosen because it is easily adaptable programming code and it could be linked with COMSOL Multiphysics FEM-program. All of the FEM-simulations were made with ANSYS Workbench 11, with one exception, because it has an efficient graphical interface and it is compatible with standard 3D-models from computer aided design programs. The hyperbolic heat conduction simulation was calculated with COMSOL Multiphysics 3.3a for the reason that the program could be modified to take into account the different form of heat conduction.

Simulations made with ANSYS

- Steady-state heating
- Bolt force
- Elastic contact
- Plastic contact
- Frequency

Simulations made with COMSOL

- Hyperbolic heat conduction

Calculations made with MATLAB

- Calculations of accuracy

The computer used was DELL Precision M70, with Intel Pentium 2 GHz processor and 1 Gb of memory.

3.3.2 Bolt forces

As the assembly is assembled by using bolts, it is convenient to study the effects of bolts and their interaction with the parts. All the assembly techniques require force to keep the quadrants together and giving the assembly features their alignment capabilities. The placement of the bolts is important to achieve the precision in every assembly method. It is important for the precision assembly that the bolts are located as close as possible to the alignment features. The ideal location is at the same point as the aligning feature, this however is not possible for the most of time. Also the fact that quadrants require bolts from two direction limits the bolt locations and the symmetry of the structure.

At this stage of the CLIC development it is convenient that the assembly method is reversible. It should be noted that the assembly force can be applied with number of different methods and even with more exact results. For example the same assembly features could be used with shrink fit. This kind of assembly could use a ring that is heated and then fitted over the cooler assembly and when the ring cools down, it would provide the necessary assembly force. However this method is not as reversible as bolts. Also soldering could be used to fix the parts together, but the reversibility issue remains and deformations would be difficult to control.

3.3.3 Connection to the next structure

The linear accelerator is composed of a module based structure. Each module includes all that is necessary for the machine to function; vacuum, drive beam, actuators, support systems, alignment systems and accelerating structures. Each module is 2 meters long; in one module there is a maximum of four accelerating structure assemblies. The alignment precision for two meters is 10μm. The connection region between two quadrant assemblies is very sensitive considering the beam stability. The geometry can not include any sharp edges or discontinues shapes. This makes the connection region very difficult to handle. It is possible to include some shapes that do not interfere too much with the particle beam.

3.4 Effects of steady-state heating

3.4.1 Steady-state heating

As RF-fields are used to accelerate the particle beam, the high magnetic field induces electric currents to the surface of the accelerating structure. The surface currents heat up the surface very rapidly every time. The accelerator operates, with its current parameters, on a frequency of 100 Hz with a pulse length of 100 ns. This causes cycling stresses to the surface and can create a fatigue problem. As the pulse heating happens in a very short time period, the overall heating can be considered as steady-state heating. The temperature difference has been considered as 10 °C from the cell surface to the cooling. This naturally causes some thermal expansion and displacements due to thermal expansion. To evaluate the magnitude of this steady-state heating, and the displacements due to it, a simulations can be conducted with FEM-programs. Also it is convenient to determine the force required to prevent the displacement and the stresses to the structure due to this. [20, 21]

3.4.2 Hyperbolic heat conduction

The Fourier-solution for the parabolic heat conduction problem is well behaving in a region of general engineering. By nature the parabolic function carries information with infinite speed. This means that any disturbance has an immediate effect on the whole system. In general situations this has negligible effect on the results. However when transient calculations are done to determine for example the heat conduction caused by short pulsed laser, this kind of solution can cause a problem. To examine the effects of short time disturbances the heat conduction problem can be modified from its parabolic form to hyperbolic. The equation for the hyperbolic heat conduction introduces term called thermal relaxation time to the solution. Thermal heat conduction term slows down the speed of conduction in the medium, the speed of temperature change is no longer infinite, and therefore improves the model to be more realistic in nature. [22, 23]

The pulsed heating and its mechanical implications in the accelerating geometry has been previously studied by Heikkinen and Huopana [21]. This research did not considerate the possible effects of the hyperbolic heat conduction. [24]

Parabolic heat conduction

$$\alpha\nabla^2 = \frac{\partial T}{\partial t} \tag{1}$$

Hyperbolic heat conduction

$$\alpha\nabla^2 = \frac{\partial T}{\partial t} + \tau\frac{\partial^2 T}{\partial t^2} \tag{2}$$

3.5 Ultra High Vacuum

Ultra High Vacuum (UHV) defined by American Vacuum Society is pressure as low as 10^{-7} to 10^{-10} Pa. The main tasks of this kind of vacuum system is to create a vacuum as low as it is defined and keep the pressure level in the defined limits. The system can suffer from gas loads. These loads are manifested when gas from the component or chamber walls is released, air and water vapor is introduced to the system through seals and leaks or by the process itself. In a UHV the number of molecules is so low that the main interaction of the molecules are with the chamber or the parts. Molecule to molecule interaction is low. In UHV the outgasing through glass can be minimized by alumiosilicated glass. [25, 26]

As the CLIC acquires UHV to operate the quadrants must be designed so that the design includes the needs and requirements of a vacuum. This means that when generating a vacuum, the parts do not have closed spaces which can trap gas or make it more difficult to achieve a vacuum. This means avoiding pockets or closed volumes, avoiding large contact surfaces and because the parts need to be cleaned before entering the vacuum chamber also such geometries which are difficult to clean should be avoided, if possible.

3.6 Metrology

To verify the simulation and the feasibility of the designed structure, it is necesarry to use a high accuracy 3D-measuring device. The measurements must be designed simultaneously with the structure to guarantee reliable measurements of the machining accuracy. These measurements should be conducted on the individual part as well as on the whole assembly. This will give the needed results to conclude the viability and stability of the assembly and the needed tolerances

for a single part. The final structures will also be measured to quarantee quality for a high number of parts. The requirements for Contcact Measuring Machine, CMM, needs a surface which can be measured easily in the direction that does not conflict with reference measurement. The same reference should be accessible in a single part as well as in the assembly. This is not possible in all cases but should be considered, if possible. The contact measuring machine used in the measurements is Ferranti Merlin 750, with a Renishaw sensor and the contact sphere has a radius of 0,25 mm with a force of 0,1N. The accuracy of the machine is $\pm 3\mu$m.

3.6.1 Error sources

Measurement

Random errors are always a part of any measurement made. Usually the errors are small and can appear either positive or negative. These errors are inflicted by parameters that cannot be either defined or controlled that effect the outcome of the measurement.

Systematic errors, compared to the random errors, commonly occur on a certain area of measurement range. Usual causes for such errors are system disturbance and the effect of environmental inputs. Because of the reoccurring nature, these kind of errors, after being recognized, can be disregarded or eliminated from the measurement. [27]

Temperature

The current design length of single quadrant is 250 mm. This means that a single degree change in temperature can cause 4 μm change in length. This induces tight environmental control to the accelerator as well as to the machining and other preparations. The temporary heat that generates from the interaction of the tool and the material, can be very high. Machining will have to be done by using environmental control that includes the cooling liquids as the surrounding air temperature to avoid thermal effects to the structure during machining. [28]

Human

As the human element in measurements and in design is the most unpredictable and many cases unavoidable there are few things that consider mentioning. The most of human errors are unavoidable and must be accepted as part of any design and measurement. There are many errors which can occur. In measurements the technological advances in measuring techniques has lowered the participation of man to the measurement. Most of the measurement are complicated and carried out in closed environments and then calculated in computers. The human factor can play a role in interpretation of the results or preparation of the measurement sample. Calibration is still important for various measurements and can cause errors. Errors can also occur for example in missed order of magnitude. Also the input data that non-specialist interpreters as valid, can been seen by a specialist to be invalid. Also a common problem is conveying information form person to person, when mostly misunderstandings happen. [29]

3.6.2 Tolerance analysis

Forming the equations for the assemblies

To have comparable data on each assembly is essential when choosing the final assembly technique. There has not been a way to show that the intended accuracy has emerged from the design and that the measured data corresponds the design on a deeper level. To create such a system that can connect the design process and the measurements from the final assembly is essential when determining the success of the design.

To create this kind of evaluating system that includes tolerances of the desired shapes and constraints, a system was developed. The beam axis was chosen to be the main alignment feature, from which the deflections of the result, would determine the effectiveness of each design. In this case the previous three cases are considered and compared. [30]

Created MATLAB-code

The calculations involving accuracy are made with MATLAB-code (Attachment A, A.2, A.3). The structure of the calculation is visible in figure 9. As the calculations are a simplification of the real structure, the calculations consider only a two part assembly. It should also be noted, that the simulated geometry is presumed to be rigid and no deformations to the parts occur. The input values for the calculations are the tolerance level of manufacturing, geometrical locations of the alignment features and the number of geometries to be calculated. From these inputs, a random error is generated within the limits of the given tolerance level. This error is then inserted to the locations of the alignment feature, which can be pins, spheres and shapes. Every method has its own specified error source. After this the points which then define the axis are calculated. This loop is then repeated as many times as the input values define. From this data a deviation is the calculated and the graphical representation is generated. By comparing the data it can be resolved which assembly method gives out the best performance, in this simplified case.

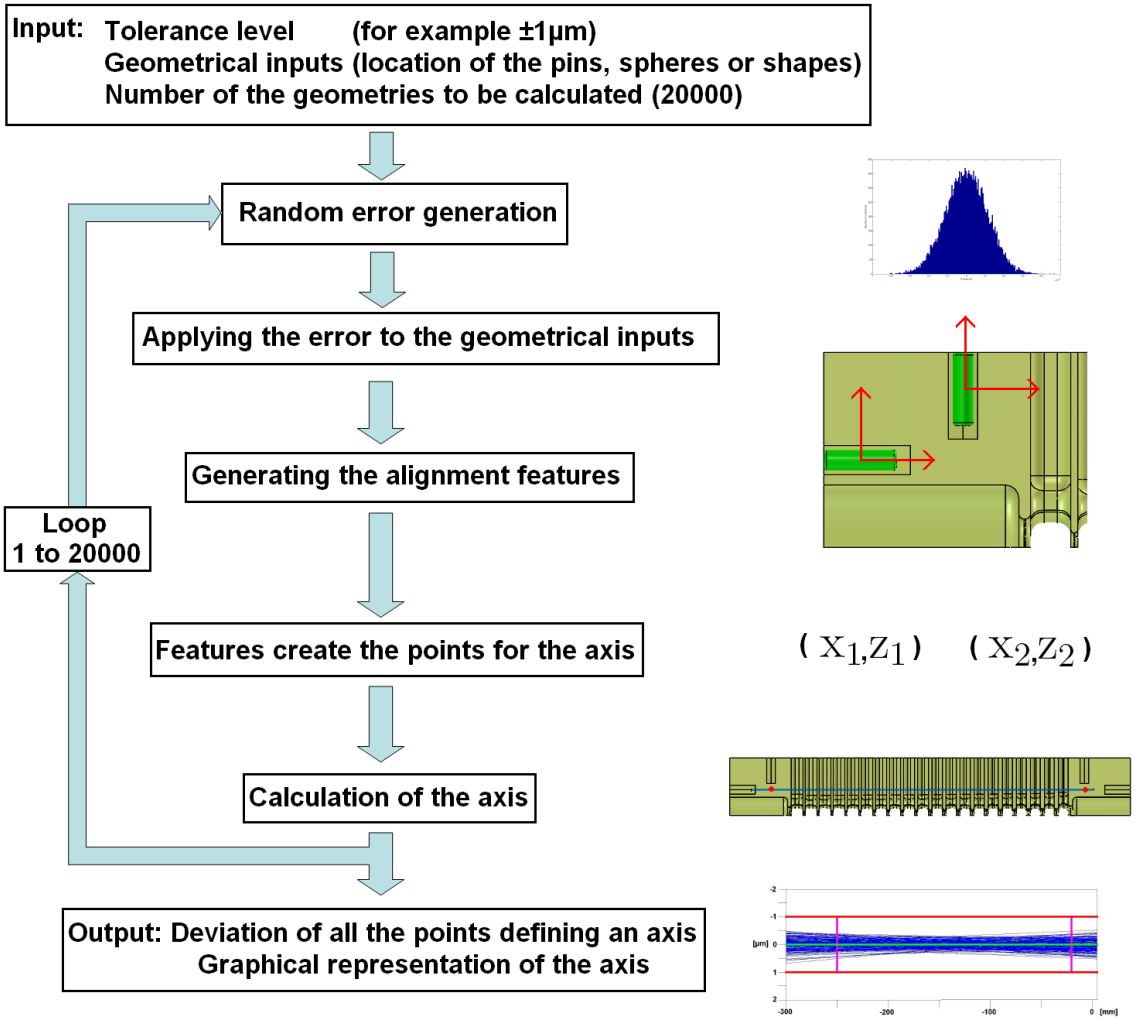

Figure 9. The structure of the calculation

3.7 Machining aspects

The high tolerance requirements of the parts are a big concern and have been under a lot of studying recent years. As the high precision assembly is very dependent on the manufacturing accuracy of a single part, there must be effort to solve the problems considering machining accuracy. The main idea to use these kind of quadrant structures is to avoid using another type of manufacturing, diamond turning, which is compared to be expensive. However, the 5 and 6-axis milling is on its limits, and best result of the test structures, considering accuracy, have been close to $\pm 5\mu$m. Also, there has been some evidence considering the machining that the techniques used suffer from systematic errors, which are thought to be the result of inaccurate tool measurement and tool wear and tear. The alignment techniques can not provide a proper alignment if the machining errors are too great. Also the surface quality and 3D-shape tolerances are very high, in the iris-region shape accuracy should lie between $\pm 1\mu$m and surface roughness Ra 0.1. For planar parts the tolerance is easier to achieve. As the assemplies use planar surface in the alignement, the planarity and perpendicular of the machine, is also an issue. For example with grinding it is possible to have very small cutting depths and achieve the micron accuracy required. It is also required to take into consideration the vibrations, stiffness and cooling of the machine itself. [31].

Tool

The most persistent error that has occurred in the machining testing has been the tool error that occurs when machining three dimensional shapes. When a high accuracy and surface quality are demanded, it is clear to use down milling. This improves the quality of the surface and the shape tolerances. However, when using only one milling direction the geometry of the tool and the accurate measurement of the tool diameter, usually the ball-end tool is used, the dimensions of the tool are critical. When machined the tool is usually pre-measured, static or dynamic measurement, and after this the tool will be moved to the reference point. After this the milling starts keeping the values considering the tool geometry and dimensions locked. This effects the result of the machining. When a periodic symmetric shape is machined the side of the tool that has been measured and referenced produces good quality. However, the other side of the tool has

the effect to be in the wrong position compared to the reference. Therefore, the other side of the milled surface usually has errors. Also the geometrical shape of the ball milling tool can vary and this has an effect to the accuracy of the fillets. [31, 32]

Tool wear clasifications according to M. C. Shawn. [33]

1. Adhesive wear.
2. Abrasive wear.
3. Diffusion wear.
4. Fatigue.
5. Microchoppiing.
6. Gross fracture.
7. Plastic deformation.

Adhesive wear happens when interacting surfaces come in contact and form bonds. Bonds can be stronger than the strength of the materials. This can cause material particles to transfer from one material to another. Abrasive wear happens by chip formation. This happens when another material is harder than the other. Diffusion wear can happen when surface velocities are low and surface temperatures are high. This environment can make solid state diffusion possible. [33–35]

3.8 FEM-simulations as part of design

Finite Element Method (FEM) has become more and more accessible for designers and manufacturers, because of the increased computer capability and software design. The user interfaces have become more accessible and easy-to-use, its not only the experts who now can benefit from the wide ranging possibilities of simulating structures and making design changes before prototypes. That said, it should also be noted that even though the programs are clear to use, it is still required to have basic knowledge of the physical phenomenon before the results can be trusted. Also there are still areas in many fields that can not be simulated with these easy-to-use programs.

The mathematical basic concept is based on virtual work or on the minimum total potential energy principle. FEM limits the structure in question to smaller and more easier to manage sections, which are called elements. These elements have similar mathematical and physical properties and are connected to their neighboring elements or boundaries. Elements form the mesh. The nature of FEM is not exact but by increasing the number of elements more and more accurate results are available at the expense of computer calculation time. Most common mechanical phenomena do not require very fine mesh to give a reasonable and acceptable answer. By keeping the solution time reasonable, the designer can simulate multiple ideas or concepts before choosing the final design. This gives advantage in time and costs, which are both useful and usually more or less connected.

FEM-simulations are ideal for predetermining mechanical phenomena of different structures, when it is needed to understand the behavior of the structure thoroughly and before manufacturing. These decreases significantly the costs of prototypes and helps the designer to have a feel about the structures properties. This also gives more ground for different choices which now can have more than a feeling or experience to relay on, even though both are always helpful when design something new.

Basic formulation of fininite element model

The basic approach to the function of finite element method in mechanical environment is through strains, stresses, forces and displacements. Let us consider a basic case of plane stress to clarify the process. A finite element, e, is a three noded triangular element with nodes i,j and k. The following equations use the same notation as Zienkiewicz. [36] The displacements can be defined in any part of the element by $\mathbf{u}$, which can be approximated with vector $\hat{u}$, as follows: [36,37]

$$\mathbf{u} \approx \hat{u} = \begin{bmatrix} N_1 & 0 & N_2 & 0 & N_3 & 0 \\ 0 & N_1 & 0 & N_2 & 0 & N_3 \end{bmatrix} \begin{Bmatrix} u_1 \\ v_1 \\ u_2 \\ v_2 \\ u_3 \\ v_3 \end{Bmatrix} = \mathbf{Na^e} \tag{3}$$

where N is functions of position and a^e is the nodal displacements of a single element. For plane stress, the 2D movement can be discribed as,

$$\mathbf{u} = \begin{Bmatrix} u(x,y) \\ v(x,y) \end{Bmatrix} \tag{4}$$

and for each node, i, in a element,

$$a_i = \begin{Bmatrix} u_i \\ v_i \end{Bmatrix} \tag{5}$$

The N_i, N_j, N_k are known as *shape functions*, which has a characteristic that the value of the shape fuction in its own node is one and zero in every other node.

$$N_i = (x_i, y_i) = 1 \tag{6}$$

As the displacements are defined in a element the strains can also be determined. The resulting displacements are,

$$\epsilon \approx \hat{\epsilon} = \mathbf{Su} \tag{7}$$

where $\mathbf{S}$ is a linear operator. The strains can be also defined as,

$$\epsilon \approx \hat{\epsilon} = \mathbf{Ba^e} \tag{8}$$

so that

$$\mathbf{B} = \mathbf{SN} \tag{9}$$

Now when a simple 2D plane stress is considered for the strains the following terms can be defined to describe the strains.

$$\epsilon = \begin{Bmatrix} \epsilon_x \\ \epsilon_y \\ \gamma_{xy} \end{Bmatrix} = \begin{Bmatrix} \frac{\partial u}{\partial x} \\ \frac{\partial v}{\partial y} \\ \frac{\partial u}{\partial y} + \frac{\partial v}{\partial x} \end{Bmatrix} = \begin{bmatrix} \frac{\partial}{\partial x} & 0 \\ 0 & \frac{\partial}{\partial y} \\ \frac{\partial}{\partial y} & \frac{\partial v}{\partial x} \end{bmatrix} \begin{Bmatrix} u \\ v \end{Bmatrix} \tag{10}$$

Now when the N shape functions are determined it is easy to calculate the matrix $\mathbf{B}$. To from the equation for the stresses, a linear elastic behavior is assumed. The resulting linear dependence between stresses and strains is:

$$\sigma = \mathbf{D}(\epsilon - \epsilon_0) + \sigma_0 \tag{11}$$

Where the ϵ_0 and σ_0 are initial strains and stresses, respectively, and $\mathbf{D}$ is the elasticity matrix defining the properties for the material. To solve the plane stresses,

$$\sigma = \begin{Bmatrix} \sigma_x \\ \sigma_y \\ \tau_{xy} \end{Bmatrix} \tag{12}$$

the material properties can be obtained by the known relations,

$$\epsilon_x - (\epsilon_x)_0 = \frac{1}{E}\sigma_x - \frac{\nu}{E}\sigma_y \tag{13}$$

$$\epsilon_y - (\epsilon_y)_0 = -\frac{\nu}{E}\sigma_x + \frac{1}{E}\sigma_y \tag{14}$$

$$\gamma_{xy} - (\gamma_{xy})_0 = \frac{2(1+\nu)}{E}\tau_{xy} \tag{15}$$

From this the elasticity matrix [**D**] can be solved,

$$\mathbf{D} = \frac{E}{1-\nu^2}\begin{bmatrix} 1 & \nu & 0 \\ \nu & 1 & 0 \\ 0 & 0 & (1-\nu)/2 \end{bmatrix} \tag{16}$$

Let q^e define the nodal forces which are equivalent to boundary tractions and distributed body forces in an element, so that every node has a corresponding nodal displacement a_i.

$$\mathbf{q^e} = \begin{Bmatrix} q_i^e \\ q_j^e \\ q_k^e \end{Bmatrix} \tag{17}$$

For plane stress the nodal forces are,

$$\mathbf{q_i^e} = \begin{Bmatrix} U_i \\ V_i \end{Bmatrix}^e \tag{18}$$

where U_i and V_i are force components corresponding to directions for displacements u and v, and body forces which are distributed for the whole element as components,

$$\mathbf{b} = \left\{ \begin{array}{c} b_x \\ \\ b_y \end{array} \right\} \tag{19}$$

By implementing a virtual nodal displacement to the system it is possible to find the corresponding external and internal forces and displacements. The implementation of virtual leads to nodal forces,

$$\mathbf{q^e} = \int_{V^e} \mathbf{B}^T \sigma dV - \int_{V^e} \mathbf{N}^T \mathbf{b} dV \tag{20}$$

which can be writen a linear,

$$\mathbf{q^e} = \mathbf{K}^e \mathbf{a} - \mathbf{f}^e \tag{21}$$

where,

$$\mathbf{K}^e = \int_{V^e} \mathbf{B}^T \sigma dV \tag{22}$$

and

$$\mathbf{f}^e = \int_{V^e} \mathbf{N}^T \mathbf{b} dV - \int_{V^e} \mathbf{B}^T \mathbf{D} \epsilon_\mathbf{0} dV + \int_{V^e} \mathbf{B}^T \sigma_\mathbf{0} dV \tag{23}$$

To describe the complete finite element model it is needed to present the external consecrated nodal forces $\mathbf{r}$

$$\mathbf{r} = \left\{ \begin{array}{c} r_1 \\ \\ r_2 \\ \\ \vdots \\ \\ r_n \end{array} \right\} \tag{24}$$

The boundary elements can be subject to external loading $\bar{t}$ which have the boundary face A^e. By the virtual work consideration, this results in

$$\mathbf{f^e} = -\int_{A^e} \mathbf{N}^T \bar{\mathbf{t}} dA \tag{25}$$

Now by using the previous relations it is possible to create a system of algebraic equations

$$\mathbf{Ka} + \mathbf{f} = \mathbf{r} \tag{26}$$

where

$$\mathbf{K} = \int_V \mathbf{B^T D B} dV \tag{27}$$

and

$$\mathbf{f} = \int_V \mathbf{N}^T \mathbf{b} dV - \int_A \mathbf{N}^{-T} t dA - \int_V \mathbf{B}^T \mathbf{D} \boldsymbol{\epsilon_0} dV + \int_V \mathbf{B}^T \boldsymbol{\sigma_0} dV \tag{28}$$

By following this formulation the theory of elasticity can be applied to every element. To have a large model, that consist of several individual elements, the elements must be connected. This can be done by a summation technique that connects each node to corresponding neighbour node, in a way that corresponds with the displacement directions and boundary conditions.

3.8.1 Contacts

When an objects boundary comes into a contact with another objects boundary or point the situation referred as contact problem. FEM is a very usefull way to solve these problems. In a contact the boundary conditions change; during the contact kinematic and before contact usually traction conditions. Hertzian contact is often referred as node-to-node which can be imposed to models when contact areas are small. The theory requires identification of the surfaces or points which are presumed to be in contact and suitable conditions to prevent penetration at the surface.

The contact problem is considered in non-linear finite element calculations with Lagrangian meshes. To the contact area a kinematic and kinetic conditions are added. The most important factor when considering contact simulations is the condition of impenetrability. This can not be described in a general useful way that could be implied in the model. Therefore, to replace this, there have been developed many ideas how to apply this boundary condition. The two main governing equations are the penalty method and augmented Lagrange method.

The penalty method can be described

$$F_n = k_n x_{pen} \tag{29}$$

and the augmented Lagrangian method

$$F_n = k_n x_{pen} + \lambda \tag{30}$$

where F_n is the normal force in contact, k_n the normal contact stiffness, x_{pen} the penetration and λ is the Lagrangian multiplier that effects the contact stiffness. The calculation of k_n has a high influence on the accuracy and on the converges of the problem. With a too high value it is possible that the solution does not converge because the stiffness causes changes to the state of the calculations in every iteration. In penalty case the penetration x_n should be in ideal cases zero, but as this is not possible in numeral cases, the value has to be in some small tolerance to have qualifiedly results. [38, 39]

3.8.2 Plastic deformation

As the contact simulations can show, the stress levels at each contact area are extremely high. This is directly related to the linear material model used in the calculations. When a ductile material experiences stress levels beyond yield stress of the material the material experiences plastic deformation. If the material can experience only small plastic deformations before failure, the material is called brittle [40]. To simulate the model with more realistic stresses the material model must be changed from a normal linear Hookes material to a model that has non-linear behavior. This can be done by applying the experimental material data available from stress-strain relations. With this information it is possible that the model deforms according the plastic strains and has stress levels which are more reliable. The simplest way to define material model that is non-linear, is to use so called bi-linear material model for the stress-stain relations. The begining of the stress-strain curve is in the area of normal elastic linearization and Hookes law, until the stress levels achieve the yield level. After this, the linearity changes according to another linear function, this is described by the tangent modulus. The figure 10 demonstrates the relations. After the material has yielded the further plastic deformation can be dependent on plastic strain. This is called *hardening*. [41]

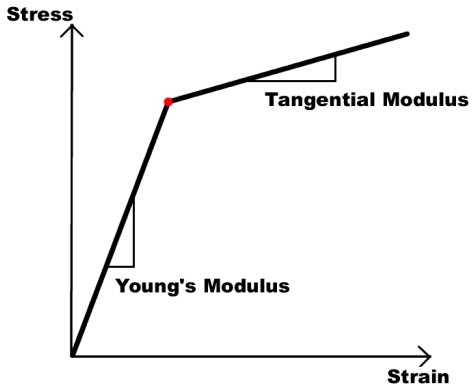

Figure 10. Bilinear material model

Chapter 4

Results

4.1 Calculations of the accuracy

4.1.1 Adapted assembly techniques

There has been two main methods of assembly so far for the quadrants. Both can be described as variation of kinematic couplings. The first idea has been to use cylindrical pins in V-grooves. Two quadrants have been aligned with four cylindrical pins, making the assembly slightly over constrained, but easier to assembly. The pins are located in the ends of the quadrants and are in 90° angle to one another, to restrict planar movement. This kind of assembly has three tolerance surfaces in each contact area; the V-groove of the first quadrant, the surface of the cylindrical pin and the surface of the second quadrant. The principle of the pin alignement is shown in figure 12. This assembly creates an axis which starts from the crossing point of the two pin axis from the other to the crossing point of the other pins in the other end, as can be seen in figure 11.

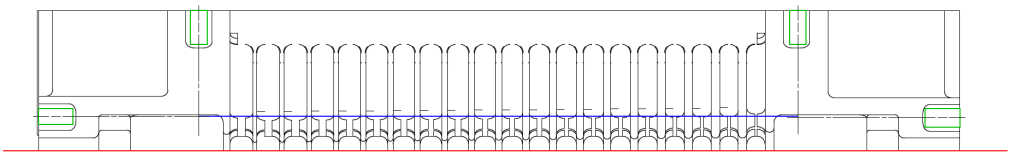

Figure 11. Using pins for the alignment

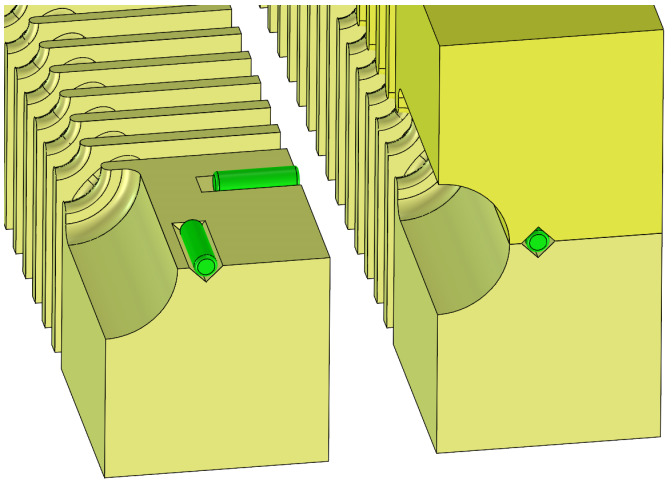

Figure 12. 3D-view of the used pins

Random numbers were used to create a change in the designed geometry inside the tolerance level. Example from the randomly generated data is presented in figure 13. As the random number are used to simulate the changes in the manufacturing tolerance. These changes cause the locations of the pins to change which results differences in a the assembly axis. The different axis are visible in the figure 14.

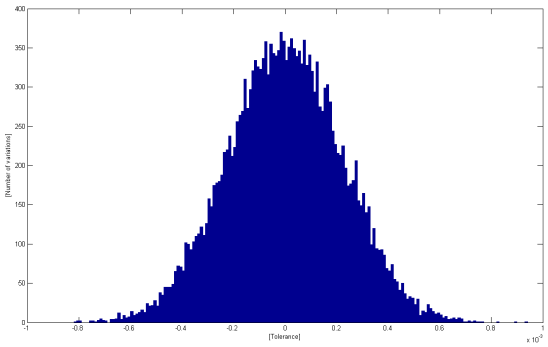

Figure 13. The randomly generated coordinates

The second method that has been used is a variation of this same scheme. The two pins in each ends has now only been replaced by one sphere. This method of two quadrants has zero degrees of freedom and is therefore perfectly constrained. The sphere in one end is placed in a tetrahedral-shaped hole, where the three

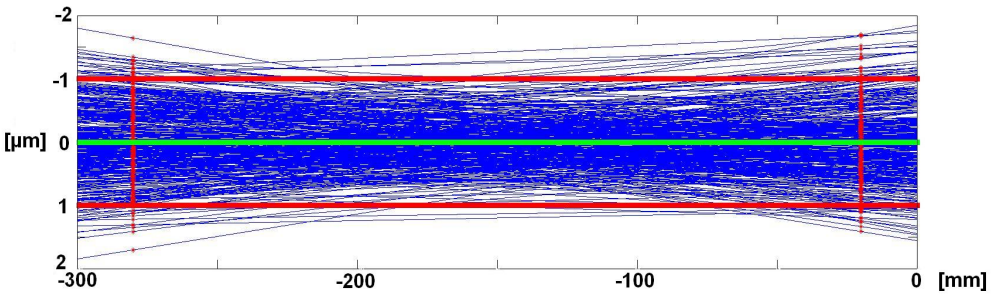

Figure 14. Using pins for the alignment

triangular surfaces restricts the movement of the sphere. The other sphere is located in the other end and it is plased in a V-groove. This spheres purpose is to prevent rotational movement of the two assembly planes. As in the previous method this one has also three tolerance surface between the three parts. The two spheres define an axis between their center points. This assembly can be seen in figure 15.

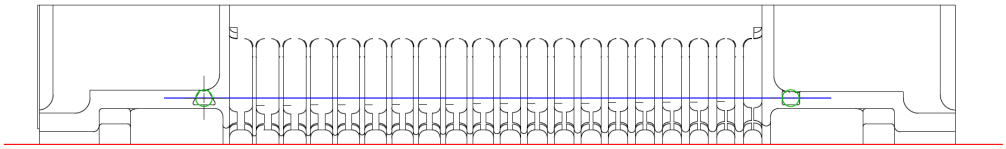

Figure 15. Using spheres for the alignment

To give clear picture how the sphere assembly behaves when the tolerance limits are set, a calculation was made with MATLAB-program. The result can be seen in figure 16. The red lines implicate the tolerance limits, green line shows the design axis and the blue lines represent assembled axis from randomly created sphere locations.

As these two applied techniques defined there own axis which can be then translated to the beam axis there is also a way to create a geometry that defines an axis that is located coincidental to the beam axis. This can be achieved with elastic averaging. To the ends of the quadrants can be machined a wave-like geometry that has an arc structure. The center points of these arcs are located at the beam axis. Between the quadrants, each part would now have only two tolerance surfaces. As the technique itself is highly over constrained the final

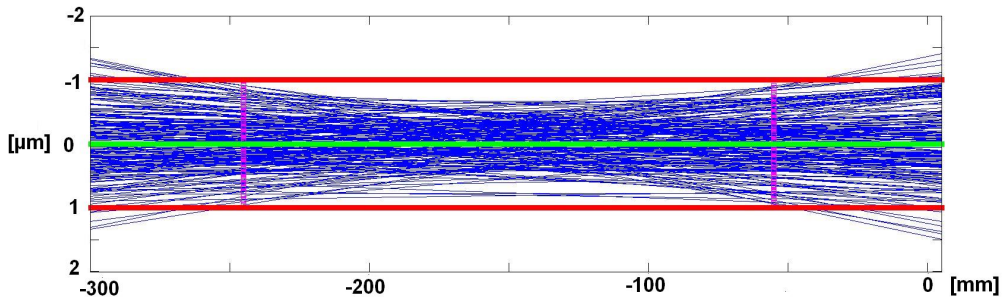

Figure 16. Tolerance analysis of spheres

accuracy comes from the multiple contacts. Through averaging the precision can be achieved with high accuracy, even though the alignment axis is outside the physical surface of the structure. This method can be seen in figure 17.

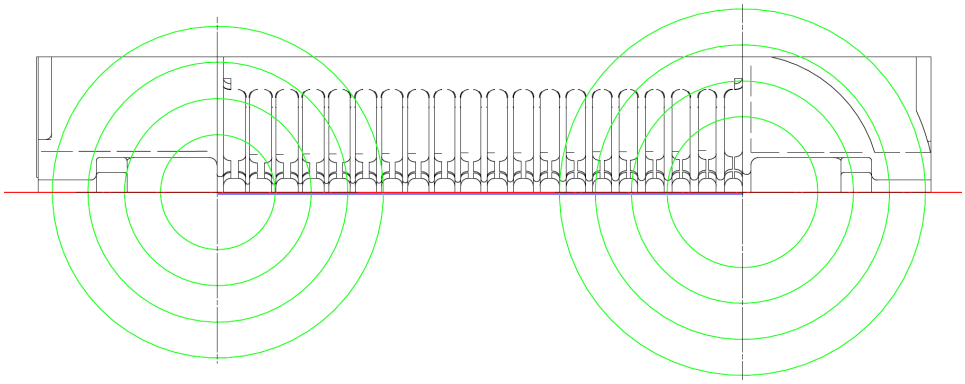

Figure 17. Using averaging shapes for the alingment

The MATLAB code A.2 which was used in the previous simulations was modified to show the same variation of parameters. The added error source is the radial error of the averaging shape that causes approximately $\frac{1}{\sqrt{2}}$ error to the location of the shapes center point. Figure 18 visualizes the example geometry in 3D. The figure 19 shows the results of the calculation. The blue lines describe the axis that were generated with a use of random numbers and average center points of the averaging shapes. The red lines show the limits of the tolerances and the green lines show the design axis. The results show that with a ± 1 μm tolerance level, using only five averaging shapes, causes the axis to set close to ± 0.5 μm. Figure 20 shows the effect of averaging shapes number to the axis. The

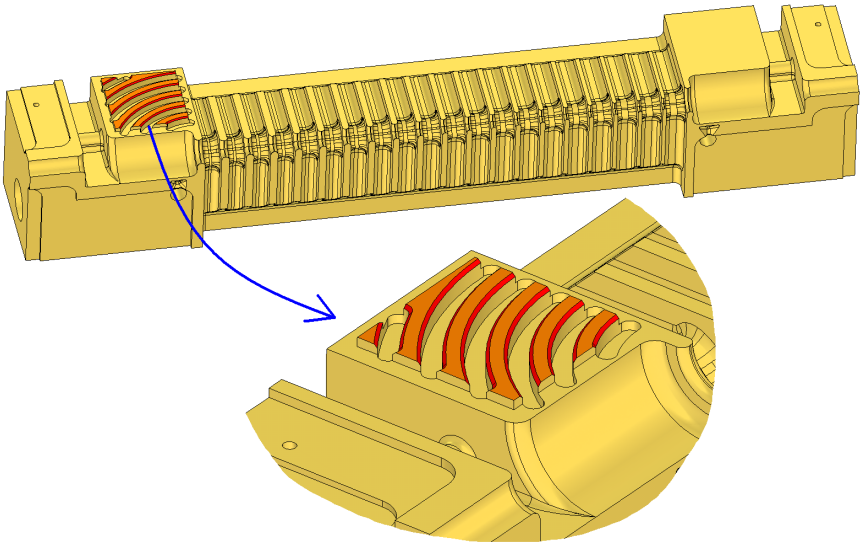

Figure 18. 3D-view of averaging feature

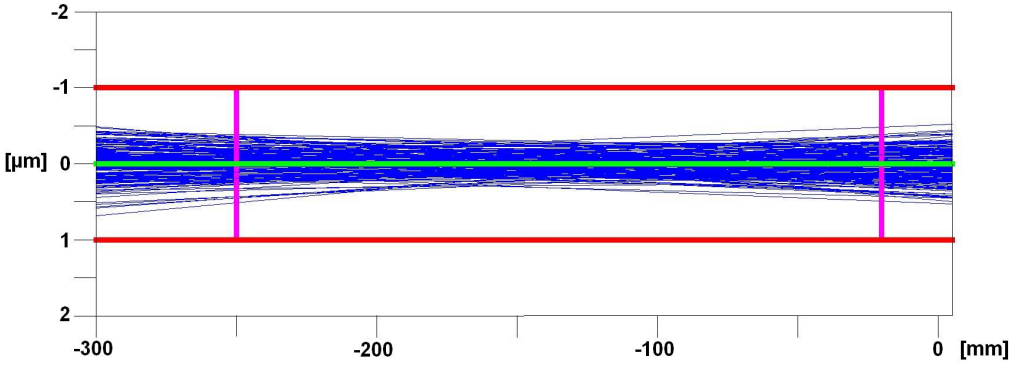

Figure 19. Tolerance analysis of average shapes

clear result of the effect can be seen when compared the effect of one averaging shape to five. [42, 43]

To evaluate the differrent methods also the standard deviations (eq. 30) were calculated from all of the assembly techniques. Keeping the tolerance level at the same values the data is comparable. Deviations from different methods can be seen in table 4. The x_1, x_2, z_1 and z_2 are the points which define the axis for each assembly.

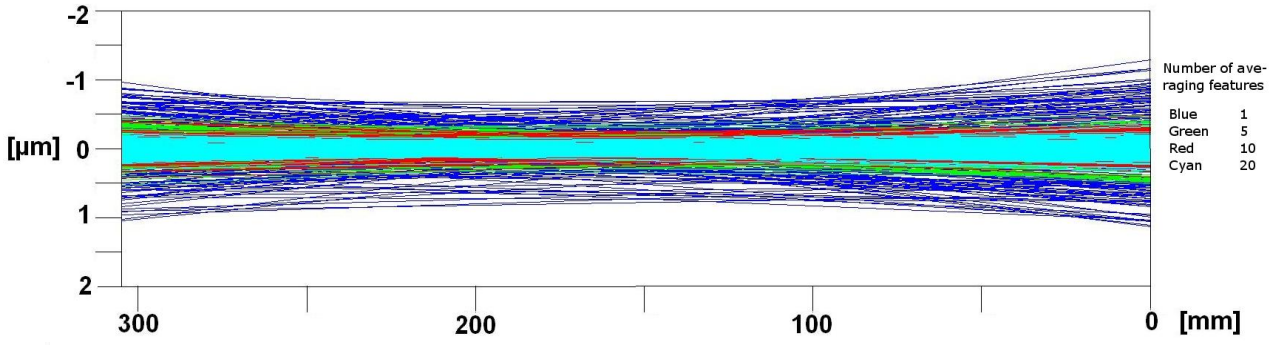

Figure 20. Effect of the number of averaging shapes to the accuracy

Standard deviation

$$\sigma_{dev} = \sqrt{\frac{\sum_{k=1}^{N}(x_k - \mu)^2}{N-1}} \tag{30}$$

Where N is the population size, μ is the mean and x_k is the kth component of the population. [44]

Table 4. Standard deviations of assembly methods

	Pins [mm]	Spheres [mm]	Average shapes [mm]
x_1	0.000601	0.000436	0.000249
z_1	0.001060	0.000384	0.000223
x_2	0.000597	0.000419	0.000207
z_2	0.000949	0.000376	0.000212

4.2 FEM-simulations

4.2.1 Steady-state heating

The simulations of steady-state heating were conducted in ANSYS Workbench environment. The temperature diffrence, ΔT, between the each cavity and the cooling channel is expected to be close 10°C (Fig. 22). This temperature diffrence was applied to the fully modeled quadrant to solve the temperature distribution and with that the thermal expansion and the mechanical influences. The boundary conditions are visible in figure 21. The mechanical boundary contion is also visible, as the structure is fixed from the top of the center iris. The result can be seen in figure 23 , which shows the displacement in x-direction. The temperature difference causes the quadrant to deform into bended shape. This is the result of higher thermal expansion in the high temperature area and the effect decreases according the temperature drop towards the cooling. It can be seen that if the quadrant is fixed from the center of the structure the ends can deform so that the distance from the beam axis is at maximum of 20 μm. It was also concluded, from the simulations, how much force is necessary to prevent this bending effect to happen. This force is applied to the end of the structure which is fixed from the middle. The force required is 26 N.

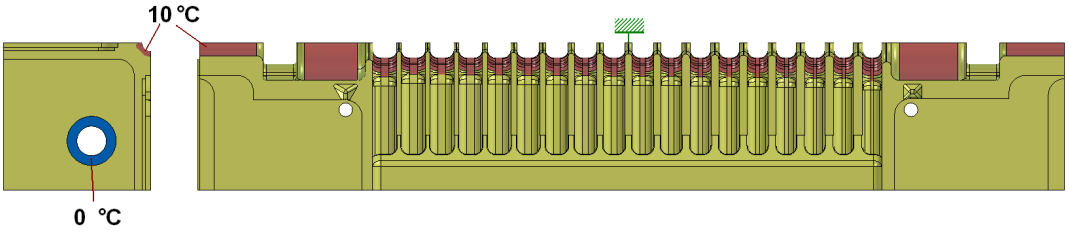

Figure 21. Boundary conditions for the simulation

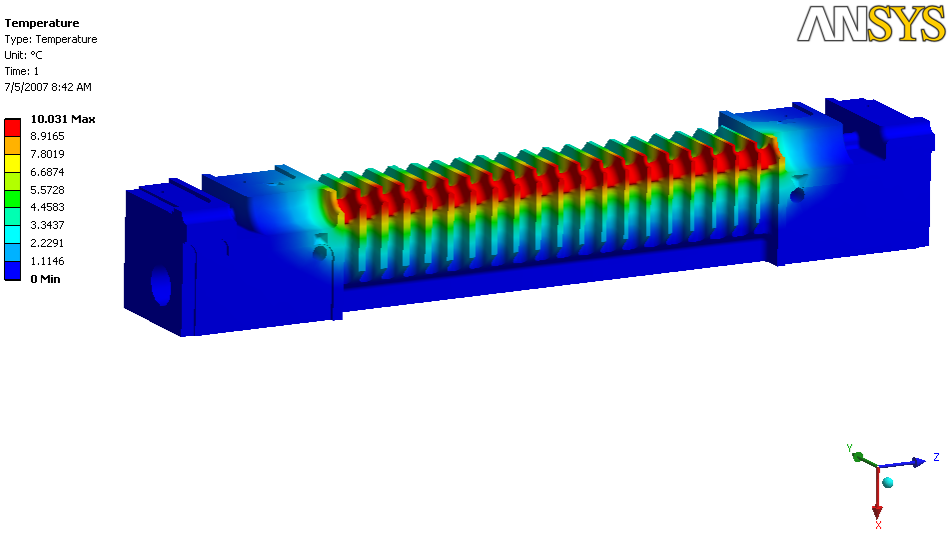

Figure 22. Temperature distribution of ΔT 10 K

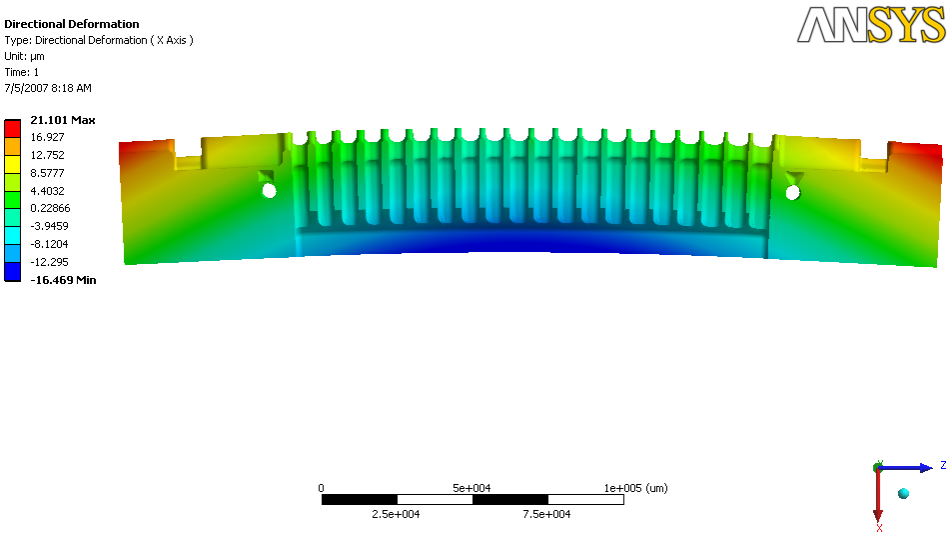

Figure 23. Deformation due to temperature distribution of ΔT 10 K in x-axis

4.2.2 Hyperbolic heat conduction implementation to FEM

The COMSOL multi-physics-program has a solver for partial differential equations which can be inputted in generic coefficient form. The hyperbolic heat conduction equation was introduces to the program and then simulated as 1D-simulation of heat conduction to a rod. The results confirmed the analytical solutions. When the pulse length is close to the thermal relaxation time the conduction of the heat slows down and this has also effect to the maximum temperature of the surface. 2D-simlation was also done by COMSOL where the use of hyperbolic equation it is possible to detect thermal waves. Speed of thermal wave is shown in equation 31. For copper the speed of thermal wave is close to 350 $\frac{m}{s}$. [45–48]

Speed of a thermal wave

$$v = \sqrt{\frac{\alpha}{\tau}} \tag{31}$$

Where τ is the thermal relaxation of the medium and α is the thermal diffusivity. Due to the magnitude of the thermal relaxation in metals and for copper, this form of heat conduction equation does not offer a significant improvements compared to the previous solutions and simulations. The thermal relaxation value in metals is around $10{\cdot}10^{-11}$s. When the accelerating geometry was simulated, the effect of the thermal relaxation was negligible and there was no mentionable impact to the maximum temperature. The solution only slightly softens the peaks of the pulse start and end. To emphasize the effect of the thermal relaxation figure 26 shows the effect of an extremely high thermal relaxation to a normalized temperature.

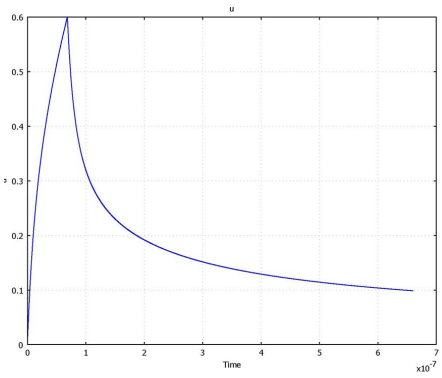

Figure 24. Parabolic heat conduction τ=0s

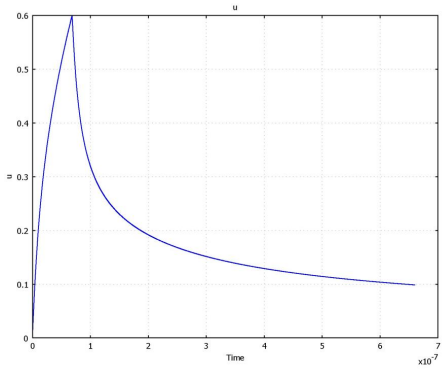

Figure 25. Hyperbolic heat conduction τ=10·10^{-11}s

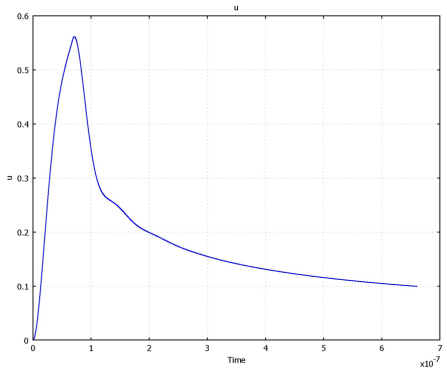

Figure 26. Hyperbolic heat conduction τ=400·10^{-7}s

4.2.3 Bolt forces

To understand the effect of the bolts and the contact and stresses resulting from tightening, a geometry as seen in figure 27 was simulated. A 1600 N tightening force was applied to the bolt in a model that represents one quarter of the whole assembly. The contact was presumed frictionless to simplify the simulation. The maximum stress levels are in the bolt and in the contact area.

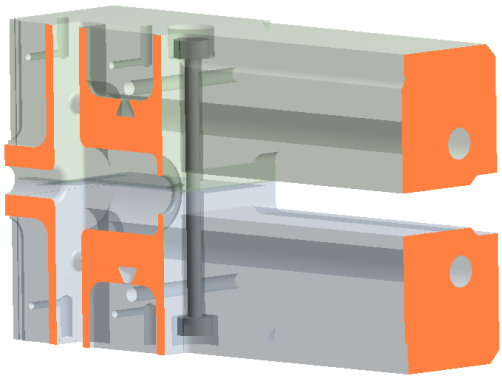

Figure 27. The simulated bolt configuration with symmetry boundary conditions highlighted

When the level of contact is evaluated, it is clear that the best contacts are near the bolts. The lower level contacts which remain on the edge of the structure are still acceptable. The visualization of the contact is visible in figure 28.

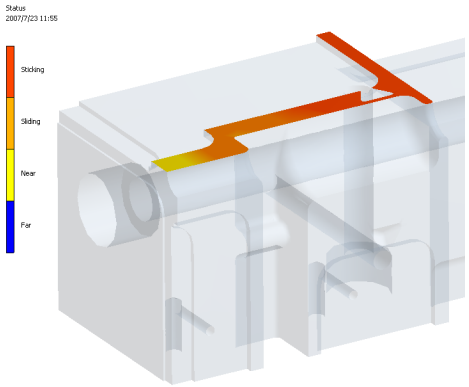

Figure 28. The level of contact between the quadrants

4.2.4 Contacts

By simulating the contacts it was possible to determine the needed force for the to close a gap from 1 μ to 20 μm. The simulation also gives the generated stress levels. The stress levels can be seen in figure 30 and the boundary conditions in which the simulation was defined are visible in figure 29.

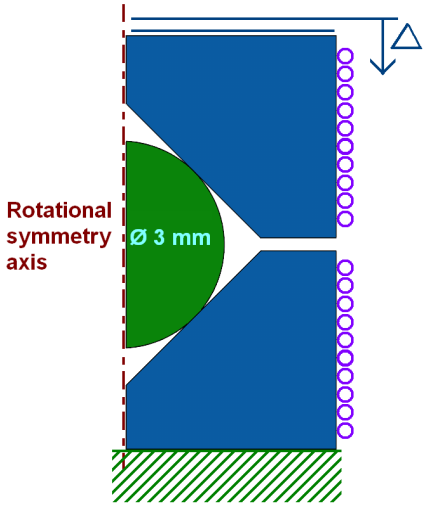

Figure 29. Boundary conditions in the simulation

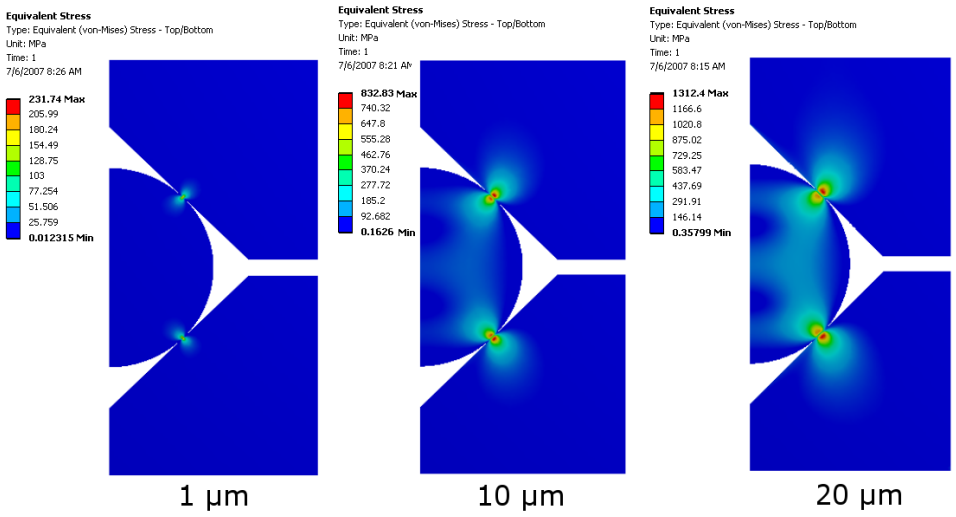

Figure 30. Stress levels for 1, 10 and 20 μm displacements

The simulations were conducted in ANSYS. The model was made as 2D and axi-symmetric to save calculation time and to improve accuracy. 3D model does not offer any aditional information. The model consist from two copper cones and one steel sphere, diameter of 3 mm. The sphere is in initial contact with the cones. The lower cone is fixed from the bottom to prevent movement of the system. The another cone has a displacement boundary condition which corresponds the needed displacement of the cone. The contact is presumed frictionless, to give clear picture of the effect of the forces to the stresses, by limiting the number of variables. This is only done to simplify the contact behavior. The calculation uses explicit calculation to improve the accuracy of the results. As the program converges, the solution gives the stress levels and the reaction force required to cause the displacement. The needed force was also simulated to specified displacements and it can be seen in figure 31 and the generated stresses are visible in figure 32. The high stress level indicates that there is a possibility for plastic deformation.

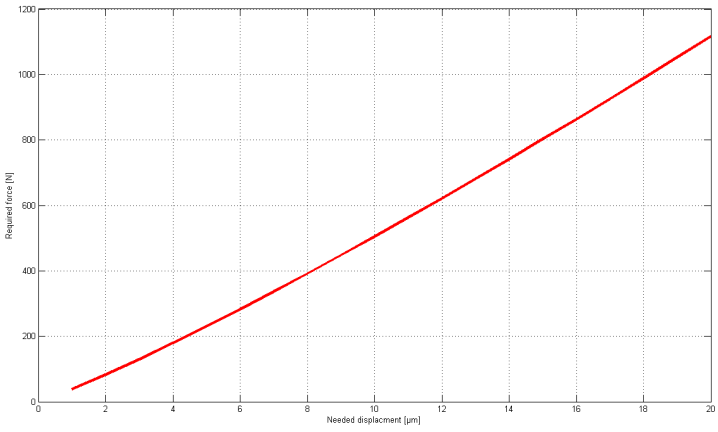

Figure 31. Needed force for the μm displacements

The reaction force needed is fairly linear for the whole displacements range. The stress levels are almost linear, except for the stress levels which corresponds for small displacements. As the sphere is forced to move more and more in each step, it should be noted that the applied force is distributed for larger area each time as the copper and steel give away elastically. The stress levels are higher in copper due to differnces in mechanical properties. Also the maximum von Mises

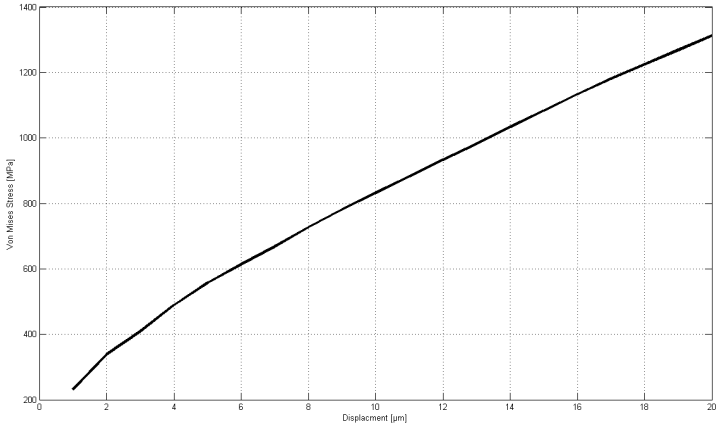

Figure 32. Stress levels caused by the displacements

stress value is always below the surface area. [49,50] This is due to then fact that von Mises is a combined value of each prime stresses including shear stress, shown in equation 32. As shear stress can not appear on a open surface the shear stress starts to grow into the material. This causes the maximum von Mises stress to be higher just below the contact surface. The detailed stress level for 10 μm can be seen in figure 33

$$\sigma_e = \sqrt{\frac{(\sigma_1 - \sigma_2)^2 + (\sigma_2 - \sigma_3)^2 + (\sigma_3 - \sigma_1)^2}{2}} \tag{32}$$

To compare the effects between the number of contacts and manufacturing tolerances in elastic averaging, a contact simulation was conducted. This was to find out the maximum force required to have contact between two bodies, when the manufacturing tolerances cause the quadrants to have imperfect contact with each other. Also friction was added to the contact surfaces to improve the evaluation of the model. This would clarify the effect that fircition has to the calculations and to the results. The resolved data was used in the MATLAB-code to evaluate each random assemblies need for force in alignment. The effect of the variation in tolerance can be calculated from the geometrical perspective as is shown in figure 34. From this it is easy to calculate the gap, δ, that is born when the maximum material condition is used for the tolerances. The results considering the effect of friction coefficient and machining tolerance to the

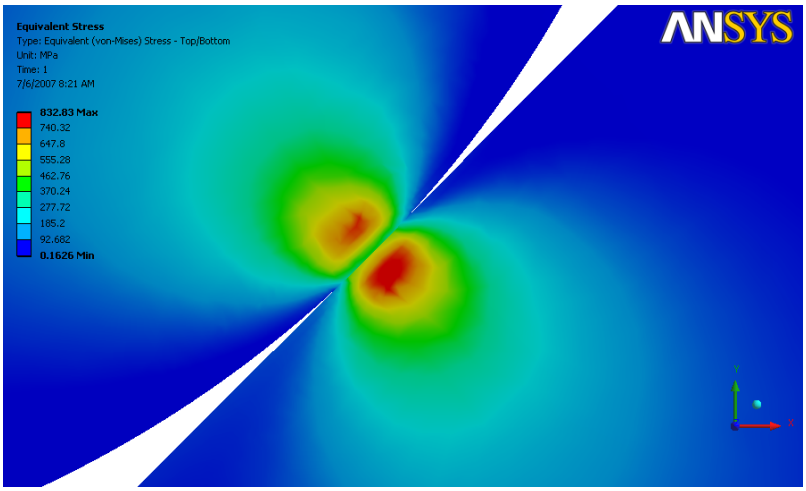

Figure 33. Detailed contact area at 10 μm displacement

required assembly force is visible in figure 36 and the used mesh and boundary conditions are visible in figure 35. The simulations were conducted as plane strain simulations. The results indicate that the effect of the friction is linear compared to the required force.

The gap between the two quadrants is:

$$\delta = \frac{\sqrt{9a\,(16R + 7a)}}{4} \tag{33}$$

Where a is the manufacturing tolerance and R (1.5 mm) is the nominal radius of the shape.

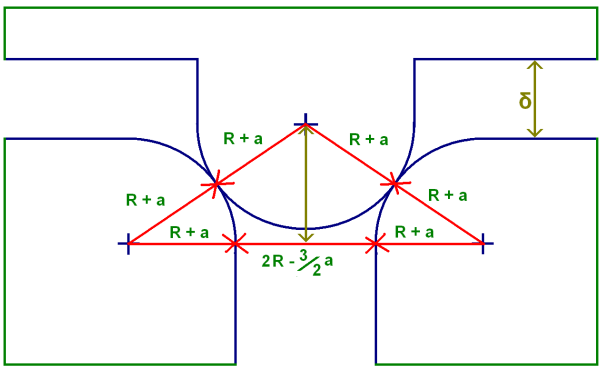

Figure 34. The simulated geometry for the tolerance relations

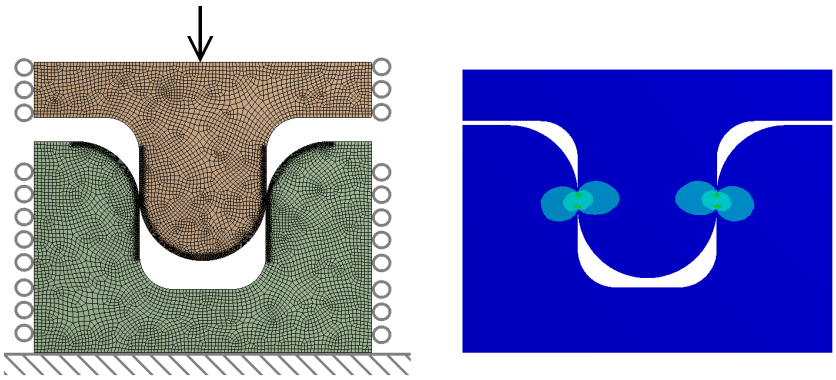

Figure 35. The mesh, boundary conditions and the resulting stress pattern

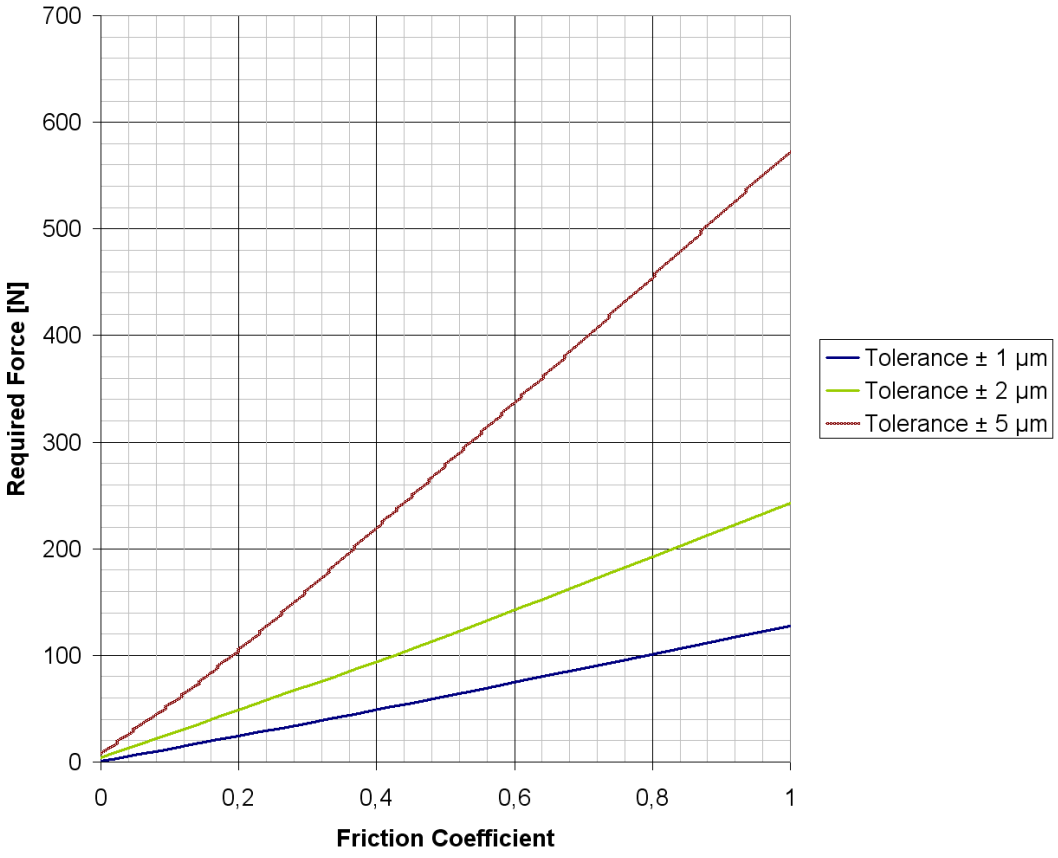

Figure 36. Friction coefficients influence to required force

4.2.5 Frequency

Every physical object has a vibration frequency that is controlled by the geometry and the material properties of the object. These frequencies are called eigenfrequencies and they are essential for mechanical design and evaluation. Knowledge of the frequencies helps the designer to avoid such frequency ranges that would excite the eigenfrequency and cause accuracy problems or in a long term scale, damage. The fundamental equation is to solve the eigenvalues of the mass and stiffness matrixes, shown in equation 34. [51]

$$\left|\left([K] - \omega^2 [M]\right)\right| = 0 \tag{34}$$

The eigenfrequencies for one quadrant were calculated to see the values of free vibrations. The ANSYS program can solve the frequencies of non-constrained object using weak spring boundary condition. The effects to the results for using this boundary condition is that the first six eigenfrequencies are the result of rigid body motion and therefore these results are not to be included as a part of the solution. The solved frequencies can be recognized quite easily, because the frequencies are usually zero or very close to zero. The effect of the weak springs can also be visible if using a boundary constrains that constrains the movement of the object in one direction and therefore reduces the degrees of freedom. The simulated eigenfrequencies for a single quadrant and for the assembly can be seen in table 5 and the visualizations of the first three shapes corresponding the eigenfrequency can be seen in figures 37–39. The assembly is presumed to behave as one body, therefore no interactions between the parts were considered.

The first and second eigenfrequency are very close to each other. When corresponding shapes of the eigenfrequencies is studied the reason for these small difference can be seen. The quadrant has almost symmetric geometry on plane that lies in 45° from the beam axis. This means that the small differences in geometry cause the quadrant to have bending shape in two directions with slightly different frequencies. The third eigenfrequency has a twisting shape along the main axis. [40]

The full four quadrant assembly was also simulated for the lowest eigenfrequencies. This was done to see the properties of the whole assembly. The single part can vibrate on its own eigenfrequency but when placed in an assembly constrained

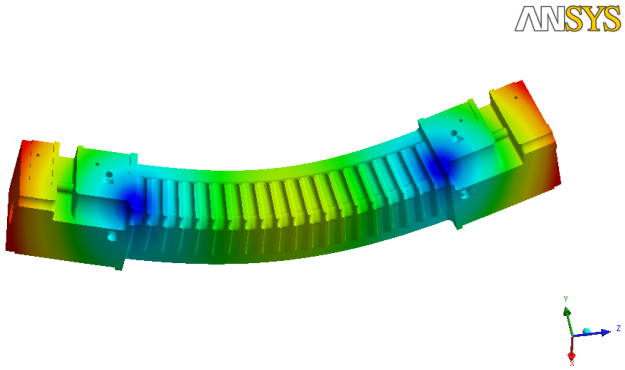

Figure 37. First eigenfrequency and shape at 1404 Hz

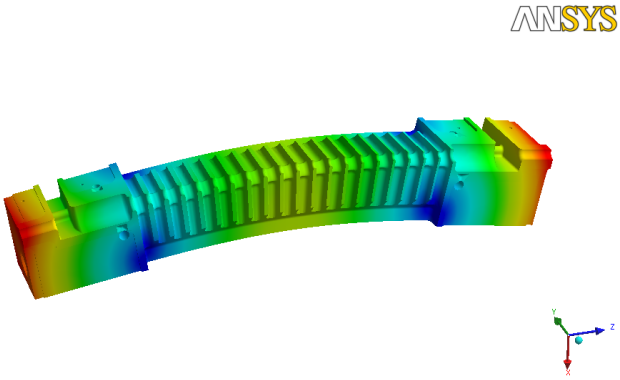

Figure 38. Second eigenfrequency and shape at 1424 Hz

with multiple contacts, the frequency of the whole assembly is combination of each individual quadrants mass and stiffness. The resulting frequencies can be seen in table 5 and the first three modes in figure 40. The similar effect is visible as it was with the quadrants second and third frequencies. The assembly's first and second frequencies are very close to each other and have a similar bending shape, but to different directions. Similar explanation for this is that the minor difference in the directional geometries with respect to the symmetry cause the effect. The first frequency is however a twisting shaped mode and in a lower frequency level.

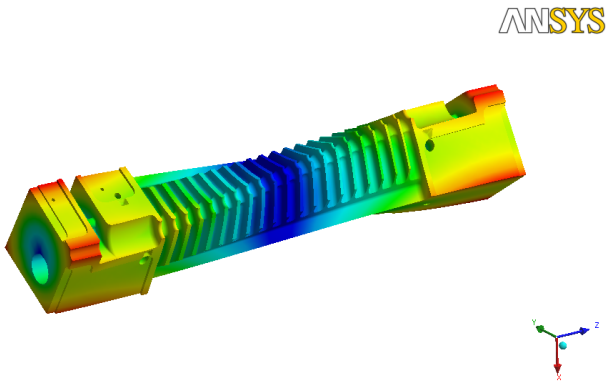

Figure 39. Third eigenfrequency and shape at 2917 Hz

Table 5. Eigenfrequencies of one quadrant and the assembly

Mode	Quadrant frequency [Hz]	Assembly frequency [Hz]
1 (DOF)	0	$1{,}7646 \cdot 10^{-3}$
2 (DOF)	0	$3{,}0194 \cdot 10^{-3}$
3 (DOF)	$7{,}7019 \cdot 10^{-4}$	$5{,}3987 \cdot 10^{-3}$
4 (DOF)	$1{,}6429 \cdot 10^{-3}$	0,20785
5 (DOF)	$2{,}7644 \cdot 10^{-3}$	0,28164
6 (DOF)	$5{,}3395 \cdot 10^{-3}$	0,80467
1.	1404,5	1688
2.	1424,7	2535,6
3.	2917,2	2566
4.	3580,2	3698
5.	3657,6	3730,3
6.	5445,8	4083,9

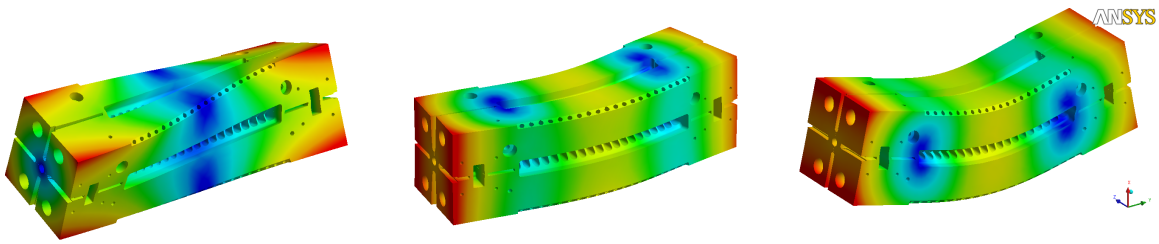

Figure 40. Assemblies first three eigenfrequencies

4.2.6 Plastic-elastic material model

As the previous contact results indicate the stress levels in contact regions are very high. When a plastic-elastic material model is introduced to the simulations the stress levels are start to have more realistic values. As the model is using the a very simple model of bilinear model to describe the model the effects of it are clearly visible and shown in figures 42 and 43. The difference is clear compared to the linear case of simulations especially in the case of the stresses. The required force to achieve the displacement is less sensitive to the material model, and therefore differs less from the linear model. This has a strong connection to the size of the contact area. Stress distribution can be seen in figure 41. The slow in crease of the stresses can be explained by isotropic hardening that the material experiences as the plastic strain grows.

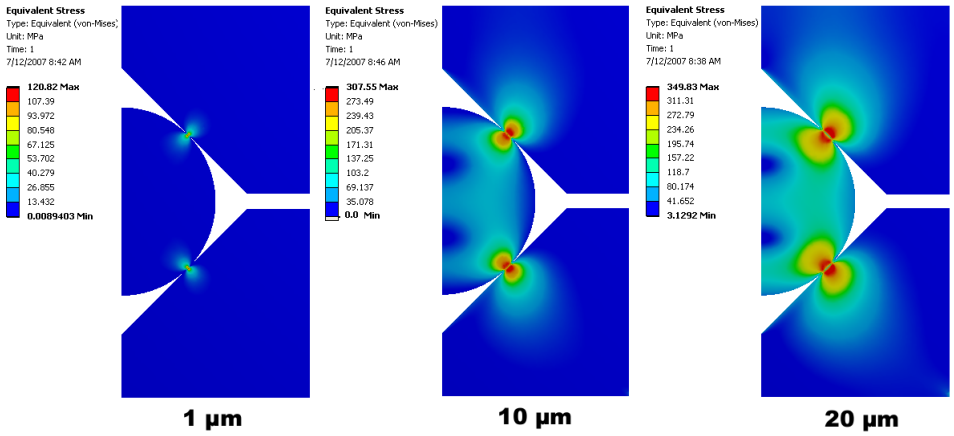

Figure 41. Stress levels when using plastic-elastic material

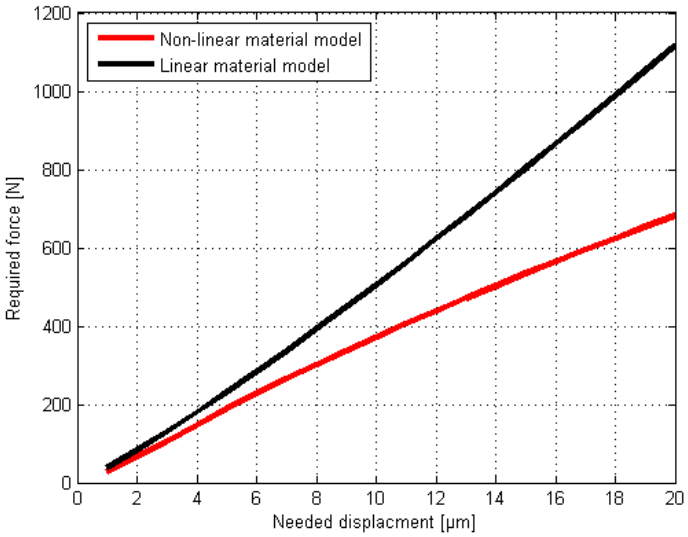

Figure 42. Force levels required to close a gap

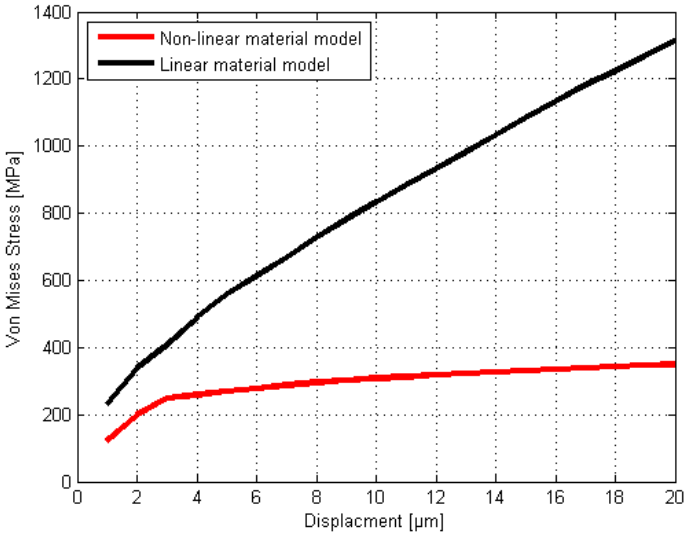

Figure 43. Stress levels required to close a gap

4.3 Effects to the design

The shape of the elastic averaging can be added to a single quadrant in away that each quadrant is the same. This can be achieved by manufacturing the needed shape to one side and making the mirror shape to the next side of the quadrant. When assembled the quadrants will have matching shapes on each side. If the shape is introduced to the design as shown in figure 44, it is very likely that the assembly can not be done by hand. The accuracy and force required would indicate an assembly system which is automated. The figure 45 shows an alternative method of applying the needed shape which can be assembled by hand. The shapes do not have the possible to lock themselves without external force. The tightening force can be applied by bolts or with some other means of compression, as close as possible to the assembly shapes. A bolt through the shapes is also acceptable.

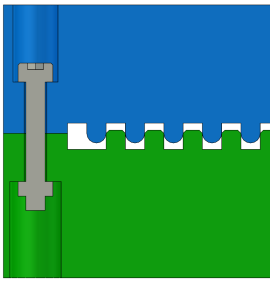

Figure 44. Possible elastic averaging shape

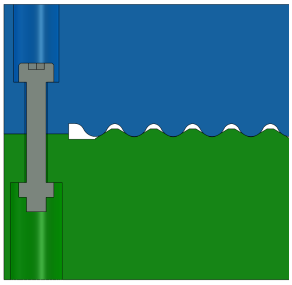

Figure 45. Elastic averaging shape

Chapter 5

Discussion

5.1 Tolerance calculations

The random tolerance input results are based on 2-dimensional model that does not fully show the final accuracy of the assembly. The 3-dimensional model can be created from these bases. Also it should be noted that the pin and the sphere assembly do not define the axis to the beam line. The axis that it is created in these methods is constrained by the location of the alignment parts and can not therefore define an axis that is outside the physical geometry of the part. The pin assembly can be modified so that the defined axis is outside of the geometry, but this would not change the tolerance sensitivity of this kind of assembly.

When the averaging features are used the number of contacts cannot be quantified very precisely. The contact surface are in contact from several places due to elasticity of the material, so the models represented here were showing the optimal line contacts of each shape. It reality the contact will not be optimal, but the number of contacts will be large than in these simulations.

The pin assembly is also more sensitive for errors in z-direction. This is due to the fact that when using pins the system is kinematicly over constrained and the calculations take this into consideration by using angular error in the locating of the pins. The axis of two pins create point that represents the definig point of the alignment axis. The angular effects therefore inflict always a directional error to the calculations.

When using the spheres in the assembly the design considers the tolerances of

the spheres. The tolerance limits of the spheres are very tight and the tolerances for the quadrants are set so, that with the maximum and minimum amount of material the sphere is always in contact. If the sphere is too large for the alignment feature the contact is designed to stay at the elastic region and respectively no plastic deformation happens.

It should also be noted that the MATLAB simulations did not include elasticity or plasticity into the calculations. The parts were considered totally rigid and independent from any material equations. The material properties did not have any effect the results and therefore the model is only describing the influence of the assembly technique and nothing more. The figure 46 shows the effect of the number of contacts to the overall error. It can be seen that the number of contacts follows very nicely $\frac{1}{\sqrt{N}}$ even with the randomized data, where N is the number of contacts.

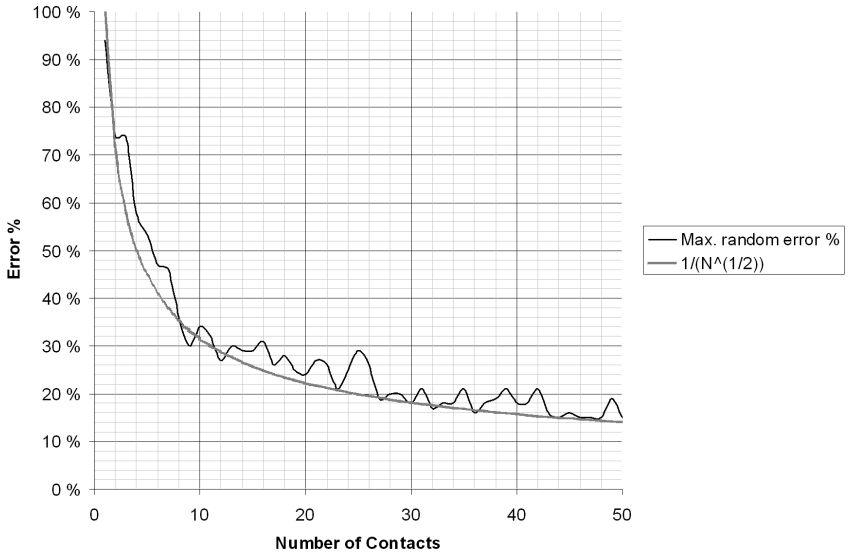

Figure 46. Number of contacts and the reduced error

The model can be used to describe different kinds of assembly methods and compare what effects the variation in the tolerance limit causes to the final model. This allows that the models can be compared with one to another and evaluated by the results. This can be done only if the sample size is constant in every calculation and the tolerances for machining are kept the same in each calculation.

5.2 FEM-simulations

The FEM-simulations were conducted on ANSYS Workbench environment with Academic Associate license. The simulations shown are the result of much iterations which was conducted to find out the best way to describe each mechanical environment in the best possible way. COMSOL Multiphysics simulation software was used in the hyperbolic heat conduction problem, mainly because it has easy access to the partial differential equations governing the problem and there were no limitations considering the input data.

Simulations considering contact were also simulated with the same ANSYS version as previously mentioned. The Workbench environment automatically finds the surfaces and induces a bonded boundary condition to every contact area. The contact areas can and were corrected represent the intended case. This does not effect the results in a way that would compromise the stress levels in each case. The result were used in a manor that would show the main areas of stress in every assembly case. The exact stress levels can be consider low to the real case of contact, but to create a true Herzian contact or applying non-linear material models would increase the calculation time with factor of three and divert the main purpose of this design process to a level of detail that is not beneficial.

Heat simulations that were done by ANSYS were steady-state analysis with constant heating properties. Transient calculations were not consider, because the effects are considered minimal. The realistic nature of pulse heating problem has already been studied by previous work and there is no need to reproduce the results although they are considered in the design. As the cooling of the structure is still in design, the level of accurate information considering the cooling parameters is low. Therefore the results on heating can be considered to be only guiding for the design to have a proper direction.

5.3 Machining and metrology

As there were no prototypes produced in the time period of this thesis, the comments towards the manufacturing and metrology are purely general and advisory. These comments and ideas were included to the design to include as much as possible for the design to show that these points have been considered and included to the design process.

Chapter 6

Conclusions

This work has presented and evaluated three different methods of an alignment for the four quadrant assembly. To evaluate the different methods a MATLAB-code was developed which functions by randomizing the tolerances to create different assembly variations. To compare the differences of the each assembly technique a standard deviation is calculated. To have more clear perspective of the mechanical behavior of the quadrants and the assembly, number of FEM-simulations were conducted. These simulations considered the eigenfrequencies of a single quadrant and assembly, contact mechanics including friction to determine the needed assembly forces for the bolt for the kinematic and elastic averaging assemblies, steady-state temperature change was considered and simulated to have results concerning thermal expansion and also effect of the needed bolt forces were simulated.

The results indicated that when it is needed to create an assembly which can compensate manufacturing accuracy, the elastic averaging is a possible choice. The calculations show that the effect of the manufacturing tolerance is linear compared to the accuracy of the assembly. Shown in figure 47.

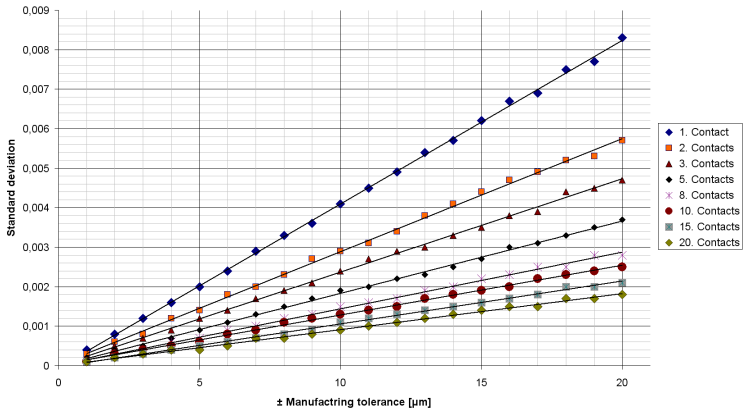

Figure 47. Manufacturing tolerances effect to deviation

The kinematic assembly with spheres results to a direct relation between the manufacturing and the assembly accuracy. The elastic averaging has the smallest deviation and it is the only method that decreases the impact of machining tolerances. The normalised results show the diffrence between the assembly methods in figure 48. As a conclusion it can be said that the elastic averaging gives the best accuracy from the studied assembly methods. The FEM-simulations provide a good basis for the understanding of the mechanical behavior. The contact analysis provided information about the needed compression forces and stresses for the kinematic sphere assembly as well as to the elastic averaging assembly. The thermal simulation shows the thermal effects for a single quadrant and indicated the needed force levels to prevent unwanted deformations. The frequency simulations give information for that is needed in the interaction of the quadrant assembly to its final module installation and indicates the frequencies that should be avoided.

For future work will be to design and manufacture a test piece and to measure the effects of assembly technique. These result will be used in this design process. The CLIC development will continue until 2010, when it feasibility of the machine will be demonstrated. This means that there should be a reliable method of assembly available in the region of two years.

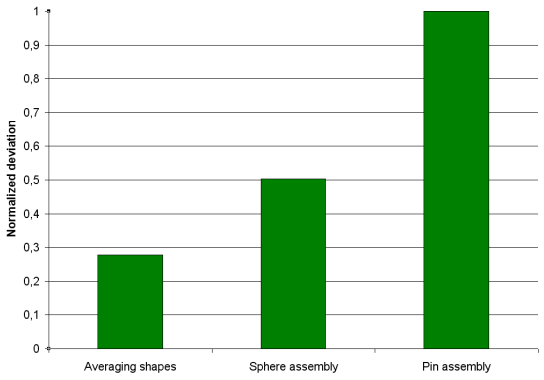

Figure 48. Normalised deviation of the assembly accuracy

Bibliography

[1] (2006) What's next at cern?, what is the lhc? CERN Publication. 16.08.2007. [Online]. Available: http://public.web.cern.ch/Public/Content/Chapters/AboutCERN/CERNFuture/WhatLHC/WhatLHC-en.html

[2] M. S. Livingston, *Particle accelerators*. New York: McGraw-Hill, 1962, 666 p.

[3] P. Waloschek, *The Infancy of Particle Accelerators, Life and Work of Rolf Wideröe*. vieweg et DESY, 2002, 18.07.2007. [Online]. Available: http://www.waloschek.de/pedro/pedro-texte/wid-e-2002.pdf

[4] (2007) Clic draft parameter list. CLIC Parameter Working Group. 05.06.2007. [Online]. Available: http://clic-meeting.web.cern.ch/clic-meeting/clictable2007.html

[5] I. H. Wilson, *The compact linear collider CLIC.*, ser. CLIC-Note. CERN, 2004, vol. 617.

[6] J. Ellis and I. Wilson. (2001, Jan.) New physics with the compact linear collider. NATURE 409, 431 - 435. 20.06.2007. [Online]. Available: http://www.nature.com/nature/journal/v409/n6818/pdf/409431a0.pdf

[7] T. P. Wangler, *Principles of RF linear accelerators*, ser. Wiley Beam Phys. Accel. Technol. New York, NY: Wiley, 1998, 382 p., 0-471-16814-9.

[8] A. Grudiev and W. Wuensch, "A newly designed and optimized clic main linac accelerating structure," *CLIC-Note 601*, Aug 2004.

[9] M. L. Culpepper, "Design and application of compliant quasi-kinematic couplings," Ph.D. dissertation, Massachusetts Institute of

Technology, Massachusetts, feb 2000, 19.06.2007. [Online]. Available: http://pergatory.mit.edu/kinematiccouplings/documents/Theses/culpepper_thesis/quasi_kinematic_couplings.pdf

[10] ——, "Constraint lecture," Massachusetts Institute of Technology Precision Machine Design lecture, fall 2001.

[11] A. H. Scolum, *Precision Machine Design.* Englewood Cliffs, New Jersey, USA: Prentice-Hall, Inc, 1992, 743 p., ISBN 0-13-690918-3.

[12] S. Awtar and E. Sevincer, "Elastic averaging in flexure mechanisms: A multi-beam parallelogram flexure case-study," in *ASME 2006 International Design Engineering Technical Conferences η Computers and Information in Engineering Conference*, Philadelphia, Pennsylvania, USA, Sept. 10–13, 2006.

[13] A. H. Slocum, "Design of three ball-groove kinematic coupling," Massachusetts Institute of Technology, MIT, Apr. 1992, 19.06.2007. [Online]. Available: http://pergatory.mit.edu/kinematiccouplings/documents/Papers/three_ball_and_groove_couplings/Design_of_Three-groove_kinematic_couplings.pdf

[14] J. Paul R. Yoder, *Opto-Mechanical System Design.* Norwalk, Connecticut, USA: CRC Press, Taylor et Francis, 2006, 835 p., ISBN 1-57444-699-1.

[15] M. L. Culpepper, "Design of quasi-kinematic couplings," *Precision Engineering*, vol. 28, pp. 338–357, 2004.

[16] E. Valtanen, *Tekniikan taulukkokirja, 14th ed.* Jyväskylä: Genesis-kirjat, 2007, 1037 p., ISBN 978-9867-27-1.

[17] J. G. Bralla, *Design for manufacturability handbook 2nd ed.* New York: McGraw-Hill, 1999, 1000 p., ISBN 0-07-007139-X.

[18] *OFE Copper*, Luvata, 2006, 23.07.2007. [Online]. Available: http://www.luvata.com/Products-and-Services/About-Copper/Copper-Grades/OFE/

[19] Valmet, *Raaka-aine käsikirja, kuparit ja kevytmetallit.* Tampere: Satapaino, 1985, 252 p., ISBN 951-95880-2-7.

[20] S. Calatroni, S. T. Heikkinen, H. Neupert, and W. Wuensch, "Status of the fatigue studies on the clic accelerating structures," CERN, Geneva, Tech. Rep. CLIC Note 678, Jul 2006.

[21] J. J. Huopana and S. T. Heikkinen, "Thermo-structural analysis of the rf-induced pulsed surface heating of the clic accelerating structures," *CLIC-Note 706*, aug 2006.

[22] M. Lewandowska and L. Malinowski, "Hyperbolic heat conduction in the semi-infinite body with the heat source which capacity linearly depends on temperature," *Heat and Mass Transfer*, vol. 33, no. 5-6, 1998.

[23] R. S. G. Heidarinejad and M. Maerefat, "Heat wave phenomena in solids subjected to time dependent surface heat flux," *Heat and Mass Transfer*, vol. DOI 10.1007/s00231-007-0259-2, 200?

[24] A. F. K. M. A. Al-Nimr and M. Hammad, "A generalized thermal boundary condition for the hyperbolic heat conduction model," *Heat and Mass Transfer*, apr 2002.

[25] J. M. Lafferty, *Foundations of vacuum science and technology.* New York, NY: Wiley, 1998, 728 p., ISBN 0-471-17593-5.

[26] M. H. Hablanian, *High-vacuum technology: a practical guide*, ser. Mechanical Engineering Series. New York, NY: Dekker, 1997, 551 p., ISBN 0-8247-9834-1.

[27] A. S. Morris, *Measurement and calibration requirements for quality assurance to ISO 9000*, ser. Wiley series in quality and reliability engineering. Chichester: Wiley, 1997, 387 p., ISBN 0-471-97685-7.

[28] T. Özel and E. Zeren, "Finite element modeling the influence of edge roundness on the stress and temperature fields induced by high-speed machining," *The International Journal of Advanced Manufacturing Technology*, jul 2006.

[29] C. Polak, T.A. Pande, *Engineering Measurements - Methods and Intrinsic Errors.* John Wiley et Sons, 1999, 12.07.2007. [Online]. Available: http://www.knovel.com/knovel2/Toc.jsp?BookID=922&VerticalID=0

[30] A. S. et all., "A new approach to statistical geometrical tolerance analysis," *The International Journal of Advanced Manufactruring Technology*, vol. 15, no. 3, mar 1999.

[31] E. J. A. Armarego, *The machining of metals.* New Jersey: Englewood CLiffs, 1969, 473 p.

[32] M. Taborelli, "Structure fabrication techniques and possibilities," in *The X-Band Accelerating Structure Design and Test-Program Workshop*, jun 2007, geneva, CERN.

[33] M. C. Shaw, *Metal cutting principles*, ser. Oxford Ser. Adv. Manufacturing. Oxford: Clarendon Press, 1984, 594 p., ISBN 0-19-859020-2.

[34] *HMS, High Speed Milling*, Sandvik Coromant, aug 2004, 12.07.2007. [Online]. Available: http://www.coromant.sandvik.com/au

[35] P. L. B. Oxley, *The mechanics of machining : an analytical approach to assessing machinability.* Horwood: Chichester, 1989, 242 p., ISBN 0-7458-0007-6.

[36] O. C. Zienkiewicz and R. L. Taylor, *The finite element method v.2, Solid mechanics.* Oxford: Butterworth, 2000, vol. 2, 459 p., ISBN 0-7506-5055-9.

[37] I. Elishakoff and Y. Ren, *Finite element methods for structures with large stochastic variations*, ser. Oxford texts in applied and engineering mathematics. Oxford: Oxford Univ. Press, 2003, 260 p., ISBN 0-19-852631-8.

[38] B. M. Ted Belytschko, Wing Kam Liu, *Finite Elements for Nonlinear Continua and Structures.* Wiley, 1996, 650 p., ISBN 0-471-98773-5.

[39] N. Kikuchi, *Contact problems in elasticity : a study of variational inequalities and finite element methods.* Philadelphia: Siam, 1988, 495 p., ISBN 0-89871-202-5.

[40] *ANSYS Worckbecnh 11.0 Analysis Guide*, ANSYS INC., 2006.

[41] D. R. J. Owen, *Finite elements in plasticity : theory and practice.* Swansea: Pineridqe Press, 1980, 594 p., ISBN 0-906674-05-2.

[42] D. M. Etter, *Engineering problem solving with MATLAB*, ser. MATLAB curriculum series. London: Prentice-Hall, 1997, 329 p., ISBN 0-13-520891-2.

[43] D. P. Landau and K. Binder, *A guide to Monte Carlo simulations in statistical physics*. Cambridge: Cambridge Univ. Press, 2000, eBook, ISBN 0511129459.

[44] J. Drake, P., *Dimensioning and Tolerancing Handbook*. McGraw-Hill, 1999, 10.07.2007. [Online]. Available: http://www.knovel.com/knovel2/Toc.jsp?BookID=330&VerticalID=0

[45] D. W. Tang and N. Araki, "On non-fourier temperature wave and thermal relaxation time," *International Journal of Thermophysics*, vol. 18, no. 2, mar 1997.

[46] *COMSOL Multiphysics Modeling Guide*, COMSOL AB, 2006.

[47] M. N. Özisik, *Heat conduction*. USA: John Wiley et Sons, 1976, 687 p., ISBN 0-471-05481-X.

[48] G. A. Mohr, *Finite elements for solids, fluids and optimization*. New York: Oxford Science Publications, 1992, 604 p., ISBN 0-19-856369-8.

[49] R. Young, W.C.; Budynas, *Roark's Formulas for Stress and Strain (7th Edition)*. McGraw-Hill, 2002, 23.07.2007. [Online]. Available: http://www.knovel.com/knovel2/Toc.jsp?BookID=475&VerticalID=0

[50] E. Pennala, *Lujuusopin perusteet*. Helsinki: Otatieto, 2002, 400 p., ISBN 951-672-297-0.

[51] M. Géradin and D. Rixen, *Mechanical vibrations theory and application to structural dynamics*. Chichester: Wiley, 1997, 425 p., ISBN 0-471-97546-X.

Appendix A

Attachment

A.1 MATLAB m-file for calculation the average shape tolerances

```
%*********************************************************************
%****** Calculation of random axis for kinematic pin assemnly  *******
%*********************************************************************

for J=1:200;

    %Inputing the manufacturing tolerances in z and x-axis
    MaTollZ = 0.001;
    MaTollX = 0.001;
    MaTolla = 0.0001;

    N = 1; %Size of the random vector

    %Design coordinates for the spheres 1 & 2
    P1z = -10;
    P1x = 20;
    P2z = -20;
    P2x = 40;
```

```
P3z = -240;
P3x = 40;
P4z = -250;
P4x = 20;

%Calculation of the crossection z = tan(alpha)* x + b
alpha1 = (pi/2) - (((MaTolla * rand(N))) - ((MaTolla) * rand(N)));
alpha2 = (((MaTolla * rand(N))) - ((MaTolla) * rand(N)));
alpha3 = (((MaTolla * rand(N))) - ((MaTolla) * rand(N)));
alpha4 = (pi/2) - (((MaTolla * rand(N))) - ((MaTolla) * rand(N)));

b1 = P1z-tan(alpha1)*P1x;
b2 = P2z-tan(alpha2)*P2x;
b3 = P3z-tan(alpha3)*P3x;
b4 = P4z-tan(alpha4)*P4x;

Sp1z = (cos(alpha1)*sin(alpha2)*b1-sin(alpha1)*cos(alpha2)*b2)/...
        (cos(alpha1)*sin(alpha2)-sin(alpha1)*cos(alpha2));
Sp1x = (cos(alpha1)*cos(alpha2)*(b1-b2))/(cos(alpha1)*sin(alpha2)...
        -sin(alpha1)*cos(alpha2));
Sp2z = (cos(alpha3)*sin(alpha4)*b3-sin(alpha3)*cos(alpha4)*b4)/...
        (cos(alpha3)*sin(alpha4)-sin(alpha3)*cos(alpha4));
Sp2x = (cos(alpha3)*cos(alpha4)*(b3-b4))/(cos(alpha3)*sin(alpha4)...
        -sin(alpha3)*cos(alpha4));

%Applying the random changes for the coordinates through the tolerances

RSp1z = Sp1z - (((MaTollZ * rand(N))) - ((MaTollZ) * rand(N)));
RSp1x = Sp1x -(((MaTollX * rand(N))) - ((MaTollX) * rand(N)));
RSp2z = Sp2z - (((MaTollZ * rand(N))) - ((MaTollZ) * rand(N)));
RSp2x = Sp2x - (((MaTollX * rand(N))) - ((MaTollX) * rand(N)));

AveSp1z = average(RSp1z);
AveSp1x = average(RSp1x);
```

```
    AveSp2z = average(RSp2z);
    AveSp2x = average(RSp2x);

    %Equation of line by two points
    x = 0:0.1:40;
    z = RSp1z + ((RSp2z - RSp1z)/(RSp2x - RSp1x))*(x-RSp1x);

    %Plotting the random axis
    plot(z,x);
    plot(RSp1z,RSp1x,'r*');
    plot(RSp2z,RSp2x,'r*');

    %Ploting the input points
    plot(P1z,P1x,'rs');
    plot(P2z,P2x,'rs');
    plot(P3z,P3x,'rs');
    plot(P4z,P4x,'rs');

    %Defining the plot
    xmin = P1x - 2 * MaTollX;
    xmax = P1x + 2 * MaTollX;
    axis([-300 0 xmin xmax]);

    xlabel('[mm]');
    ylabel('[mm]');
    hold on

    xx1(J)=(RSp1x);
    zz1(J)=(RSp1z);
    xx2(J)=(RSp2x);
    zz2(J)=(RSp2z);
end

%Plotting the tolerance limits and the desing axis
```

```
t = -320:0.1:10;
plot(t,20.001,'rs','LineWidth',1);
plot(t,19.999,'rs','LineWidth',1);
plot(t,20,'gs','LineWidth',1);

%Standard deviation
Dx1 = std(xx1);
Dz1 = std(zz1);
Dx2 = std(xx2);
Dz2 = std(zz2);
disp(['  Deviation x1 = ' num2str(Dx1)]);
disp(['  Deviation z1 = ' num2str(Dz1)]);
disp(['  Deviation x2 = ' num2str(Dx2)]);
disp(['  Deviation z2 = ' num2str(Dz2)]);
```

A.2 MATLAB m-file for calculation the average shape tolerances

```
%************************************************************************
%***   Calculation of random average shape locations effect       ******
%************************************************************************

for J=1:200;

    N = 5; %Number of averaging shapes

    %Inputing the manufacturing tolerances in z and x-axis
    MaTollZ = 1/1000;
    MaTollX = 1/1000;

    %Design coordinates for the spheres 1 & 2
    Sp1z = -20;
```

```
Sp1x = 0;
Sp2z = -250;
Sp2x = 0;

%Radial error in shapes
rz1 = 1/(sqrt(2))*(((MaTollZ * rand(N))) - ((MaTollZ) * rand(N)));
rx1 = rz1;
rz2 = 1/(sqrt(2))*(((MaTollZ * rand(N))) - ((MaTollZ) * rand(N)));
rx2 = rz2;

%Applying the random changes for the coordinates through the tolerances

RSp1z = Sp1z - (((MaTollZ * rand(N))) - ((MaTollZ) * rand(N))) - rz1;
RSp1x = Sp1x -(((MaTollX * rand(N))) - ((MaTollX) * rand(N))) - rx1;

RSp2z = Sp2z - (((MaTollZ * rand(N))) - ((MaTollZ) * rand(N))) - rz2;
RSp2x = Sp2x - (((MaTollX * rand(N))) - ((MaTollX) * rand(N))) - rx2;

AveSp1z = average(RSp1z);
AveSp1x = average(RSp1x);
AveSp2z = average(RSp2z);
AveSp2x = average(RSp2x);

%Equation of line by two points
x = -40:0.1:40;
z = AveSp1z + ((AveSp2z - AveSp1z)/(AveSp2x - AveSp1x))*(x - AveSp1x);

 %Plotting the random axis
 plot(z,x);
 plot(RSp1z,RSp1x,'ms');
 plot(RSp2z,RSp2x,'ms');
 xmin = Sp1x - 2 * MaTollX;
 xmax = Sp1x + 2 * MaTollX;
 xlabel('[mm]');
```

```
     ylabel('[mm]');

     axis([-300 5 xmin xmax]);

     hold on

    xx1(J)=(AveSp1x);
    zz1(J)=(AveSp1z);
    xx2(J)=(AveSp2x);
    zz2(J)=(AveSp2z);

end

%Plotting the tolerance limits and the desing axis
t = -320:0.1:10;
plot(t,0.001,'rs','LineWidth',1);
plot(t,-0.001,'rs','LineWidth',1);
plot(t,0,'gs','LineWidth',1);
     xlabel('[mm]');
     ylabel('[mm]');
%Standard deviation
Dx1 = std(xx1);
Dz1 = std(zz1);
Dx2 = std(xx2);
Dz2 = std(zz2);
disp(['  Deviation x1 = ' num2str(Dx1),' sample ']);
disp(['  Deviation z1 = ' num2str(Dz1)]);
disp(['  Deviation x2 = ' num2str(Dx2)]);
disp(['  Deviation z2 = ' num2str(Dz2)]);
```

A.3 MATLAB m-file for calculation the sphere location tolerances

```
%************************************************************************
%******   Calculation of random sphere locations effect       **********
%************************************************************************

for J=1:200;

    %Inputing the manufacturing tolerances in z and x-axis
    MaTollZ = 0.001;
    MaTollX = 0.001;

    %Design coordinates for the spheres 1 & 2
    Sp1z = -55;
    Sp1x = 15;
    Sp2z = -245;
    Sp2x = 15;

    %Applying the random changes for the coordinates through the tolerances
    N = 0; %Number of random trials
    RSp1z = Sp1z - (((MaTollZ * rand(1))) - ((MaTollZ) * rand(1)));
    RSp1x = Sp1x -(((MaTollX * rand(1))) - ((MaTollX) * rand(1)));
    RSp2z = Sp2z - (((MaTollZ * rand(1))) - ((MaTollZ) * rand(1)));
    RSp2x = Sp2x - (((MaTollX * rand(1))) - ((MaTollX) * rand(1)));

    %Equation of line by two points
    x = 0:0.1:40;
    z = RSp1z + ((RSp2z - RSp1z)/(RSp2x - RSp1x))*(x-RSp1x);

    %Plotting the random axis
    plot(z,x);
```

```
    plot(RSp1z,RSp1x,'ms');
    plot(RSp2z,RSp2x,'ms');
    xmin = Sp1x - 2 * MaTollX;
    xmax = Sp1x + 2 * MaTollX;
    xlabel('[mm]');
    ylabel('[mm]');
    axis([-300 5 xmin xmax]);
    hold on

    xx1(J)=(RSp1x);
    zz1(J)=(RSp1z);
    xx2(J)=(RSp2x);
    zz2(J)=(RSp2z);
end

%Plotting the tolerance limits and the desing axis
t = -320:0.1:10;
plot(t,15.001,'rs','LineWidth',1);
plot(t,14.999,'rs','LineWidth',1);
plot(t,15,'gs','LineWidth',1);

%Standard deviation
Dx1 = std(xx1);
Dz1 = std(zz1);
Dx2 = std(xx2);
Dz2 = std(zz2);
disp(['  Deviation x1 = ' num2str(Dx1)]);
disp(['  Deviation z1 = ' num2str(Dz1)]);
disp(['  Deviation x2 = ' num2str(Dx2)]);
disp(['  Deviation z2 = ' num2str(Dz2)]);
```